DESIGN OF OPTIMAL PUMPING SCHEDULES TO ENHANCE OIL AND GAS PRODUCTION FROM UNCONVENTIONAL RESERVOIRS

A Thesis

by

PARTH BHANDAKKAR

Submitted to the Office of Graduate and Professional Studies of
Texas A&M University
in partial fulfillment of the requirements for the degree of

MASTER OF SCIENCE

Chair of Committee,	Joseph Sang-Il Kwon
Committee Members,	M. M. Faruque Hasan
	Kan Wu
Head of Department,	Arul Jayaraman

May 2020

Major Subject: Chemical Engineering

Copyright 2020 Parth Bhandakkar

ABSTRACT

Hydraulic fracturing is a technique extensively used in the oil and gas industry, where water, proppant (sand) and additives are injected into unconventional reservoirs to enhance the recovery of shale hydrocarbon. Because of complex fracture growth in naturally fractured unconventional reservoirs, the ultimate goal of hydraulic fracturing operation should be changed from achieving a desired fracture geometry to maximizing the total fracture surface area (TFSA) for given fracturing resources, as it will allow more drainage area available for oil recovery. Unfortunately, there are no such techniques available to develop pumping schedules to maximize the TFSA for given fracturing resources in naturally fractured unconventional reservoirs. Motivated by this, we developed a model-based pumping schedule by utilizing a recently developed unconventional complex fracture propagation model called Mangrove describing complex fracture networks by accounting for interaction between hydraulic fractures and natural fractures. We demonstrated that by using the proposed control scheme, the TFSA can be greatly enhanced which will increase the cumulative shale oil production volume, compared to the existing pumping schedules.

Although some previous studies have developed pumping schedules that maximize gas production for a single-size proppant, there are very few studies that consider the effect of varying proppant diameters across pumping stages on shale gas production. Motivated by this, we conducted a sensitivity analysis and extended the previous pumping schedule by considering multi-size proppant for simultaneously propagating multiple fractures to maximize shale gas production from unconventional reservoirs. Since the size of injected proppant particles determines the average propped surface area (PSA) and average fracture conductivity (FC), we developed a framework called Sequentially Interlinked Modeling Structure (SIMS) to predict the average PSA, average FC and cumulative shale gas production volume for a given pumping schedule. Then, we used the SIMS framework to obtain a multi-size proppant pumping schedule that maximizes shale gas production. Finally, we demonstrated that obtained pumping schedule gives a gas production volume greater than the values obtained from the existing pumping schedules which consider only single

size proppant.

DEDICATION

To aai, baba and Atharva

ACKNOWLEDGMENTS

First and foremost, I would like to thank my principal investigator, Dr. Joseph Sang-Il Kwon for his guidance throughout. His creative ideas, insightful suggestions, and necessary criticisms have helped me stay focused and divert my energy in the right direction. I cannot be more thankful to him for making me, what I am today. I would also like to extend my sincerest gratitude towards my committee members Dr. M. M. Faruque Hasan and Dr. Kan Wu for their necessary help.

Next, I would like to take this opportunity to thank Dr. Prashanth Siddhamshetty for being an excellent mentor, guide and friend. I am highly grateful to him for helping me passionately whenever required, both within and outside the research group. I would also like to thank my research colleagues Mr. Abhinav Narasingam, Mr. Mohammed Saad Faizan Bangi, Mr. Dongheon Lee and Mr. Hyun-Kyu Choi for all the help that they have provided from time to time.

I would also like to extend my gratitude to my dearest friends and colleagues at Texas A&M, especially Niranjan, Bhavana, Debopamaa, Rushant and Suvesh. I feel lucky to have had you all beside me during this memorable journey. Thank you for making this an experience that it truely was.

Last, but not the least, I would like to extend my profound gratitude to my mom, dad and brother for their unconditional support and encouragement. None of this would have been possible without them.

CONTRIBUTORS AND FUNDING SOURCES

Contributors

This work was supervised by a thesis committee consisting of Dr. Joseph Sang-Il Kwon [principal advisor] and Dr. M. M. Faruque Hasan of the Department of Chemical Engineering and Texas A&M Energy Institute, and Dr. Kan Wu of the Department of Petroleum Engineering.

All work for Chapter 2 of this thesis was performed by the student, with some guidance from the research group members. All other work conducted for the thesis was completed by the student independently.

Funding Sources

Financial support from the National Science Foundation (CBET-1804407), the Department of Energy (DE-EE0007888-10-8), the Texas A&M Energy Institute, and the Artie McFerrin Department of Chemical Engineering are gratefully acknowledged.

NOMENCLATURE

ROM	Reduced Order Model
MOESP	Multivariable Output Error State Space
ANN	Artificial Neural Network
SIMS	Sequentially Interlinked Modeling Structure
PSA	Propped Surface Area
TFSA	Total Fracture Surface Area
FC	Fracture Conductivity
DDM	Displacement Discontinuity Method
NPV	Net Present Value
UFM	Unconventional Fracture Model
MPC	Model Predictive Controller

TABLE OF CONTENTS

Page

LIST OF FIGURES

FIGURE Page

LIST OF TABLES

TABLE Page

1. INTRODUCTION

Hydraulic fracturing is a stimulation technique to enhance the oil and gas production that typically involves injecting water, proppant (sand), and additives under high pressure into unconventional reservoirs. Hydraulic fracturing, commonly known as 'fracking', is used to create new fractures in the existing rock, and also increase the size, spread, connectivity and conductivity of existing fractures. This technique is commonly used in low-permeability rocks like shale and tight sandstone to increase oil and/or gas flow to a well from petroleum-bearing unconventional reservoirs. The importance of using proppant in the hydraulic fracturing operation in unconventional reservoirs has been discussed in detail by Fredd et al. [2]. Although hydraulic fracturing stimulations using vertical wells in conventional reservoirs have been in practice for over six decades, it is the current practice of horizontal drilling in unconventional reservoirs that has led to its massive popularitiy in the oil and gas industry.

Shale revolution in the United States started in the beginning of the 21st century from Barnett Shale reservoir, located in the central-north Texas. The United States eventually surpassed Russia to become the largest global producer of natural gas and oil in 2014. In the United States itself, as per the data obtained from Annual Energy Outlook 2019 released by U.S. Energy Information Administration, the production of dry gas from unconventional reservoir has increased from just 5.7 trillion cubic feet in 2000 to over 26 trillion cubic feet in 2019.

In this thesis, we develop pumping schedules that maximize shale oil and gas production from unconventional reservoirs. In Chapter 2, we develop model-based pumping schedule to enhance shale oil production from naturally-fractured unconventional reservoirs. In Chapter 3, we develop multi-size proppant pumping schedule to enhance shale gas production volume considering simultaneously propagating multiple fractures.

2. ENHANCING TFSA IN NATURALLY FRACTURED UNCONVENTIONAL RESERVOIRS VIA MODEL PREDICTIVE CONTROL

2.1 Introduction

Natural fractures (discontinuities in shale rock formations) are commonly observed in most of the unconventional reservoirs using advanced fracture diagnostic techniques such as microseismic monitoring, core samples and outcrops [3, 4, 5, 6]. These natural fractures will interact with hydraulic fractures, divert fracture propagation and result in a complex fracture geometry [7, 8]. The resulting complex fracture geometry in naturally fractured unconventional reservoirs plays a major role in recovering oil, subsequently determining the performance of the well. Therefore, it is very important to consider the interaction between hydraulic fractures and natural fractures to optimize hydraulic fracturing treatments in naturally fractured unconventional reservoirs.

The three possible scenarios when a propagating hydraulic fracture interacts with a natural fracture are shown in Fig. 2.1 [7]. First, the hydraulic fracture will continue to propagate like a planar fracture in the same direction by crossing the natural fracture (Fig. 2.1a). Second, the hydraulic fracture will divert into the natural fracture and will re-initiate its propagation at the natural fracture's tip (Fig. 2.1b). Third, the diverted hydraulic fracture will re-initiate at some weak point along the natural fracture (Fig. 2.1c).

The interaction between hydraulic fractures and natural fractures has been studied experimentally and numerically by many researchers [9, 10, 11, 12, 13]. To analyze complex fracture networks, the wire-mesh model [14, 15] and the discrete-fracture-network model [16] are generally used, in which a complex fracture geometry is approximated by the orthogonal grid pattern of hydraulic fractures. However, these approaches ignore the mechanisms of how natural and hydraulic fractures interact. Olson and Taleghani [17] developed a model to describe multiple, non-planar, pseudo-3-dimensional (P3D) fracture propagation in naturally fractured unconventional

*Reprinted with permission from "Enhancing total fracture surface area in naturally fractured unconventional reservoirs via model predictive control" by Siddhamshetty, P., Bhandakkar, P., and Kwon, J. S. 2020. *Journal of Petroleum Science & Engineering*, 184, 106525, Copyright 2020 Elsevier.

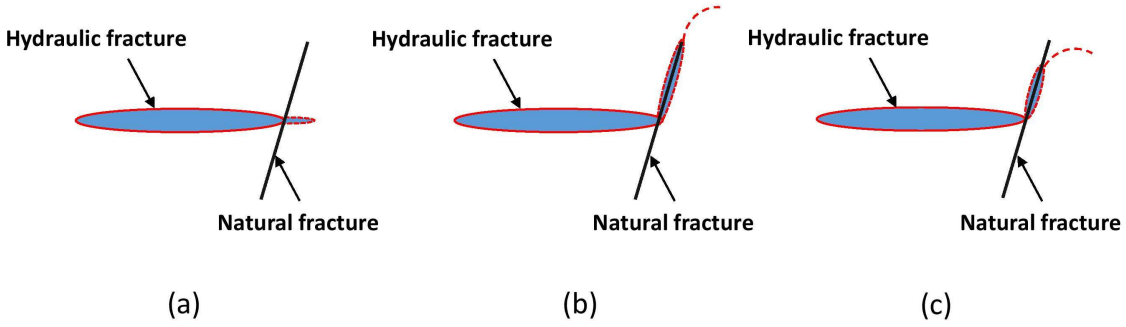

Figure 2.1: Possible scenarios when a hydraulic fracture interacts with a natural fracture.

reservoirs, but the model did not consider pressure drops in fractures due to fluid flow. Budyn et al. [18] and Keshavarzi et al. [19] modeled the hydraulic fracture propagation using an extended-finite-element-method (XFEM) model to analyze the natural and hydraulic fracture interaction. However, both of these XFEM models are two-dimensional (2D) and do not consider the three-dimensional (3D) effects such as the evolution of fracture height. Recently, Wu and Olson [20] developed a complex hydraulic fracturing model by employing the 3D displacement discontinuity method, which was computationally efficient. In this model, the hydraulic fracture propagation direction during its interaction with natural fractures was determined using a crossing criterion by modifying the extended Renshaw and Pollard criterian [11, 21]. However, this model did not consider the proppant transport in naturally fractured unconventional reservoirs. Recently, Weng et al. [22] developed an unconventional fracture model (UFM) by considering height growth, fracture deformation, fluid flow and proppant transport in naturally fractured unconventional reservoirs to simulate complex fracture network. Based on the UFM, Schlumberger developed a hydraulic fracture simulator called Mangrove which is an engineered stimulation package available in Schlumberger Petrel platform. In this work, we have used Mangrove to simulate the complex fracture growth in naturally fractured unconventional reservoirs.

In hydraulic fracturing, achieving an optimal fracture geometry is important as it will maximize the oil production rate from unconventional reservoirs [23]. Recently, several studies have been

conducted to compute the fracturing fluid pumping schedule by developing real-time model-based feedback control strategies and to achieve an optimal fracture geometry [1, 23, 24, 25, 26, 27, 28, 29, 30, 31, 32]. However, they did not consider natural fractures, which may result in a complex fracture geometry. Because of this complex fracture growth behavior, the ultimate goal of hydraulic fracturing in naturally fractured unconventional reservoirs should be changed from achieving a desired fracture geometry to maximizing the total fracture surface area (TFSA) for given fracturing resources such as water, proppant, viscosifying agent, etc. This will increase the drainage area, thereby enhancing the overall oil production rate in naturally fractured unconventional reservoirs [33]. Therefore, the pumping schedule computed using existing control schemes cannot be directly applied to naturally fractured unconventional reservoirs. Motivated by this, in this chapter, we develop a model-based pumping schedule to maximize the TFSA by utilizing Mangrove to describe complex fracture growth in naturally fractured unconventional reservoirs.

This chapter is organized as follows: High-fidelity model formulation using Mangrove is described in Section 2.2. In Section 2.3, we present a sensitivity analysis to show the importance of maximizing the TFSA in naturally fractured unconventional reservoirs. In Section 2.4, we present existing pumping schedule design techniques and their drawbacks. In Section 2.5, we construct a reduced-order model (ROM) that describes the relationship between the manipulated input variables (i.e., flow rate of fracturing fluid and proppant concentration at the wellbore) and output variable (i.e., TFSA) using the data generated from Mangrove. Next, we design a Kalman filter utilizing the available measurement to estimate unmeasurable ROM states. In Section 2.6, we present a model-based feedback control framework to compute the fracturing fluid pumping schedule that maximizes TFSA with given resources. In Section 2.7, we present the closed-loop simulation results to demonstrate that the obtained TFSA can lead to an enhanced oil production rate from naturally fractured unconventional reservoirs.

2.2 High-fidelity model formulation using Mangrove

In this section, we will discuss the UFM developed by Weng et al. [22], which considers the complex fracture growth in naturally fractured unconventional reservoirs.

2.2.1 Overview of the UFM

The UFM introduced by Weng et al. [22] has assumptions and equations very similar to that of P3D model, but solves a problem where fluid flow and rock deformation are coupled in a complex fracture network where natural fractures have to be considered. A key advantage of the UFM is that it is able to simulate the interaction of hydraulic fractures with pre-existing natural fractures. In particular, it determines whether (a) a hydraulic fracture propagates like a planar fracture in the same direction by crossing a natural fracture, (b) a hydraulic fracture is arrested when it interacts with a natural fracture, or (c) a hydraulic fracture diverts into a natural fracture and subsequently propagates along a natural fracture. In addition to the interaction between hydraulic fractures and natural fractures, the UFM also considers the interaction between adjacent fractures (i.e., the stress-shadow effect). The UFM solves a system of governing equations describing fluid flow in the fracture network, mass conversation, fracture deformation, height growth, proppant transport and fracture interaction to simulate the propagation of a complex fracture network that consists of many intersecting fractures, which are described below.

2.2.1.1 Fluid Flow equations

The local mass conservation equation at any location in the complex fracture network is given as:

$$\frac{\partial q}{\partial s} + \frac{\partial (H_{fl}\overline{w})}{\partial t} + q_L = 0 \tag{2.1}$$

$$q_L = 2h_L u_L \tag{2.2}$$

where H_{fl} is the height of a fracture at position s and time t, q denotes the local fracturing fluid flow rate, $\overline{w}$ is the average width of a fracture at position $s = s(x, y)$, and q_L is the leak-off volume rate through the hydraulic fracture wall (leak-off velocity, u_L, times leak-off fracture height, h_L), which is computed using Carter's leak-off model.

The pressure drop along a fracture branch in a complex fracture network for laminar flow of

power-law fluid can be expressed using Poiseuille law:

$$\frac{\partial p}{\partial s} = -\alpha_0 \frac{1}{\overline{w}^{2n'+1}} \frac{q}{H_{fl}} \left| \frac{q}{H_{fl}} \right|^{n'-1} \tag{2.3a}$$

and for turbulent fracturing fluid flow:

$$\frac{\partial p}{\partial s} = -\frac{f\rho}{\overline{w}^3} \frac{q}{H_{fl}} \left| \frac{q}{H_{fl}} \right| \tag{2.3b}$$

where

$$\alpha_0 = \frac{2k'}{\phi(n')^{n'}} \cdot \left(\frac{4n'+2}{n'} \right)^{n'} ; \phi(n') = \frac{1}{H_{fl}} \int_{H_{fl}} \left(\frac{w(z)}{\overline{w}} \right)^{\frac{2n'+1}{n'}} dz \tag{2.4}$$

where p is the fluid pressure, $w(z)$ denotes the fracture width as a function of depth z, f represents the fanning factor, ρ is the density of slurry, and n' and k' are the fracturing fluid power-law index and consistency index, respectively.

The fracture height and width profiles in a multi-layered formation depends on the fluid pressure, fracture toughness, in-situ stresses, layer thickness and elastic modulus of each layer. The fracture height is calculated by matching the fracture toughness to the stress intensity factors at fracture tips. Stress intensity factors K_{1u}, K_{1l} and width profile are given as follows [34]:

$$K_{1u} = \sqrt{\frac{\pi h}{2}}\left[p_{cp} - \sigma_n + \rho_f g\left(h_{cp} - \frac{3h}{4}\right)\right] + \sqrt{\frac{2}{\pi h}}\sum_{i=1}^{n-1}(\sigma_{i+1} - \sigma_i) \times \left[\frac{h}{2}\arccos\left(\frac{h-2h_i}{h}\right) - \sqrt{h_i(h-h_i)}\right] \tag{2.5a}$$

$$K_{1l} = \sqrt{\frac{\pi h}{2}}\left[p_{cp} - \sigma_n + \rho_f g\left(h_{cp} - \frac{h}{4}\right)\right] + \sqrt{\frac{2}{\pi h}}\sum_{i=1}^{n-1}(\sigma_{i+1} - \sigma_i) \times \left[\frac{h}{2}\arccos\left(\frac{h-2h_i}{h}\right) + \sqrt{h_i(h-h_i)}\right] \tag{2.5b}$$

$$w(z) = \frac{4}{E'}\left[p_{cp} - \sigma_n + \rho_f g\left(h_{cp} - \frac{h}{4} - \frac{z}{2}\right)\right]\sqrt{z(h-z)} + \frac{4}{\pi E'}\sum_{i=1}^{n-1}(\sigma_{i+1} - \sigma_i) \left[(h_i - z)\,\mathrm{arcCosh}\,\frac{z\left(\frac{h-2h_i}{h}\right) + h_i}{|z-h_i|} + \sqrt{z(h-z)}\arccos\left(\frac{h-2h_i}{h}\right)\right] \tag{2.5c}$$

where K_{1u} and K_{1l} are the stress intensity factors at the top and bottom of fracture tips, respectively, h is the fracture height, p_{cp} is fracturing fluid pressure at height h_{cp} measured from the bottom tip of the reference fracture, σ_n and σ_i are the in-situ stresses at the top and the i^{th} layer, respectively, h_i is the distance between the fracture bottom tip and top of i^{th} layer, ρ_f is the fluid density and $E' = E/(1-\nu^2)$ where E is Young's modulus, ν is Poisson's ratio.

In addition to the above equations, the following global volume balance must be satisfied at each time:

$$\int_0^t Q(t)dt = \int_0^{L(t)} h(s,t)\overline{w}(s,t)ds + \int_{H_L}\int_0^t\int_0^{L(t)} 2u_L ds dt dh_L \tag{2.6}$$

where t is the current time, $L(t)$ is the total fracture length in the hydraulic fracture network at time t and $Q(t)$ is the fracturing fluid flow rate at the wellbore. The global volume balance equation essentially signifies that the total volume of injected fracturing fluid is equal to the volumes of fracturing fluid present in the fracture network and leak-off fluid to the surrounding formation.

These equations, along with the boundary conditions stating that the fracture tip's width, net pressure and flow rate are zero, describe the fluid flow through a complex fracture network.

2.2.1.2 *Hydraulic and natural fractures interaction*

The interaction between propagating hydraulic fractures and pre-existing natural fractures is a very complex phenomenon. The modeling of this system requires consideration of various rock properties like Young's modulus, tensile strength, poisson's ratio, toughness, permeability and cohesion. It should also incorporate various fracturing fluid properties like viscosity, density and pressure. In addition to this, mechanical properties like cluster spacing and relative angle between hydraulic fractures and natural fractures also govern whether a hydraulic fracture will cross a natural fracture, dilate a natural fracture, or be arrested at a natural fracture as explained by Wu and Olson [33]. The average opening width of a fracture [35] and average pressure of a fracturing fluid in the natural fracture [36, 37] are governed by the following equations:

$$\overline{w} = 2.53 \left[\frac{Q\mu L^2}{E'H} \right]^{1/4} \qquad p_{NF}(t) = p_f \tanh\left(\sqrt{\frac{2kp_f}{\mu b_s^2}} t \right) \tag{2.7}$$

where μ is the slurry viscosity, p_f is the fracture tip's fluid pressure, p_{NF} is the fluid pressure within a natural fracture, k is the permeability of natural fracture, t is the contact time and b_s is the boundary of sliding zone as a result of contact between a natural fracture and hydraulic fracture.

2.2.1.3 *Stress shadow effects*

Stress shadow effects refer to alteration in the growth pattern of a hydraulic fracture due the presence of neighboring fractures. The disturbance from nearby fractures leads to a significant perturbation in the propagating hydraulic fracture. In this work, 2D Displacement Discontinuity Method (DDM) described by Crouch et al. [38] is used to quantify the normal and shear stresses on a fracture element due to opening and shearing displacement discontinuities. It is defined as follows:

$$\sigma_n^i = \sum_{j=1}^{N} A^{ij} C_{ns}^{ij} D_s^j + \sum_{j=1}^{N} A^{ij} C_{nn}^{ij} D_n^j \tag{2.8a}$$

$$\sigma_s^i = \sum_{j=1}^{N} A^{ij} C_{ss}^{ij} D_s^j + \sum_{j=1}^{N} A^{ij} C_{sn}^{ij} D_n^j \tag{2.8b}$$

where σ_n and σ_s are the normal and shear stresses, respectively, D_n and D_s are the opening and shearing displacement discontinuities, respectively, C^{ij} are the 2D plane-strain elastic influence coefficients and A^{ij} are the 3D correction factors introduced by Olson [39] to account for the 3D effect caused by finite fracture height.

Based on this UFM, Schlumberger developed a hydraulic fracture simulator called Mangrove which is an engineered stimulation package available in Schlumberger Petrel platform. In this work, we have used Mangrove to simulate complex fracture growth in naturally fractured unconventional reservoirs.

Remark 1. *The parameters required to set up the Mangrove simulator for a specific rock formation are reservoir thickness, Young's modulus, Poisson ratio, minimum and maximum horizontal stresses, and natural fracture properties such as length, orientation and spacing between natural fractures. The minimum horizontal stress of rock formation can be obtained from minifrac or extended leak-off test, and maximum horizontal stress is available from wellbore failure image and modeling. Rock properties such as Young's modulus and Poisson ratio can be obtained from well logs. Microseismic measurements can be used to partially predict the distribution of natural fractures by comparing the effective stimulated volume for a given distribution of natural fractures.*

2.2.2 Reservoir Simulator

Apart from simulating complex fracture networks, Mangrove can model the oil production through proppant-propped complex fractured networks. Specifically, the output from the UFM is fed as an input to the automated grid generator [40]. After establishing the production grid including a complex fracture geometry, we simulate production from an oil well in a naturally fractured unconventional reservoir using Mangrove. Then the Net Present Value (NPV) of the oil produced from the well is calculated using the following equation:

$$NPV = \int_0^T Q_{oil} r_{oil} (1+I)^{-ct} dt \tag{2.9}$$

where Q_{oil} is the oil production rate from the well, t is the elapsed time since the oil production was initiated, T is the total oil production time, r_{oil} is the oil market price, c is the time constant, and I is the money discount rate. In this work, c and I are taken as 0.1 and 1/365 (1/day), respectively.

2.3 Sensitivity analysis of complex fracture growth in naturally fractured reservoirs

During hydraulic fracture propagation in naturally fractured reservoirs, the complex fracture growth depends on in-situ stresses, rock mechanical properties, natural fracture properties and hydraulic fracture treatment parameters (e.g., fracturing fluid properties and pumping schedules). In this section, we performed sensitivity analysis on the effect of natural fracture distribution (e.g., length, orientation and spacing between natural fractures) and fracturing fluid pumping schedule (e.g., flow rate and proppant concentration injected at the wellbore) on TFSA for given rock properties (e.g., Young's modulus, Poisson ratio and in-situ stresses).

2.3.1 Effect of natural fracture distribution on TFSA

For all the simulations, we considered a single-stage hydraulic fracturing operation with three simultaneously propagating multiple fractures from the three clusters with a fracture spacing of 100 ft. We considered a total of 487200 lb proppant available for injection per stage. All the other parameters used in the simulations are given in Table 2.1.

2.3.1.1 Effect of natural fracture orientation on TFSA

The orientation of natural fractures, which is defined by the relative angle (β in Fig. 2.2) between hydraulic fractures and natural fractures, is one of the important factors affecting the final fracture geometry. As the relative angle decreases, the tendency of hydraulic fractures to cross natural fractures decreases [41]. Consequently, hydraulic fracture propagation will divert into natural fractures leading to a complex fracture geometry. In this sensitivity analysis, we considered four different relative angles (0°, 30°, 45° and 90°) with a differential stress (i.e., the difference between the maximum and minimum horizontal stresses) of 200 psi and all other parameters were kept as same of those given in Table 2.1. The total number of natural fractures, their lengths, and inter-fracture spacing were generated assuming they will follow normal distributions [42]. The statistical

Parameter	Value
Fracturing fluid flow rate	$60\ \mathrm{bbl/min}$
Stage length	$200\ \mathrm{ft}$
Reservoir thickness	$500\ \mathrm{ft}$
Young's modulus	$1.57\ \mathrm{Mpsi}$
Poisson ratio	0.35
Proppant particle density	$2640\ \mathrm{kg/m^3}$
Slick-water density	$1000\ \mathrm{kg/m^3}$
Viscosity	$0.64\ \mathrm{cp}$
Minimum horizontal stress	$4450\ \mathrm{psi}$
Maximum horizontal stress	$4650\ \mathrm{psi}$
Perforations in each cluster	12
Diameter of each perforation	$0.42\ \mathrm{in}$
Proppant mesh size	$80/100$
Diameter of proppant	$0.00647\ \mathrm{in}$
Friction coefficient	0.6

Table 2.1: Model parameters used for sensitivity studies.

parameters used to generate natural fractures with different relative angles are given in Table 2.2 and the corresponding 2D traces of fracture networks are shown in Fig. 2.3.

	Length (ft)	Spacing (ft)	Friction coefficient	Relative angles			
Average	100	50	0.6	0°	30°	45°	90°
Standard deviation	50	5	0	0°	0°	0°	0°

Table 2.2: Natural fracture distribution with different relative angles.

We observed that hydraulic fractures are unable to cross natural fractures for the four relative angles considered in this work. Instead, they diverted into natural fractures leading to a complex fracture geometry as shown in Fig. 2.3. Mangrove uses the crossing criterion developed by Chuprakov et al. [37] to predict the interaction between hydraulic fractures and natural fractures; the criterion was developed by considering the effect of in-situ stress ratio, friction coefficient, relative angle, flow rate and viscosity. As per this criterion, a fracturing fluid will leak into natural

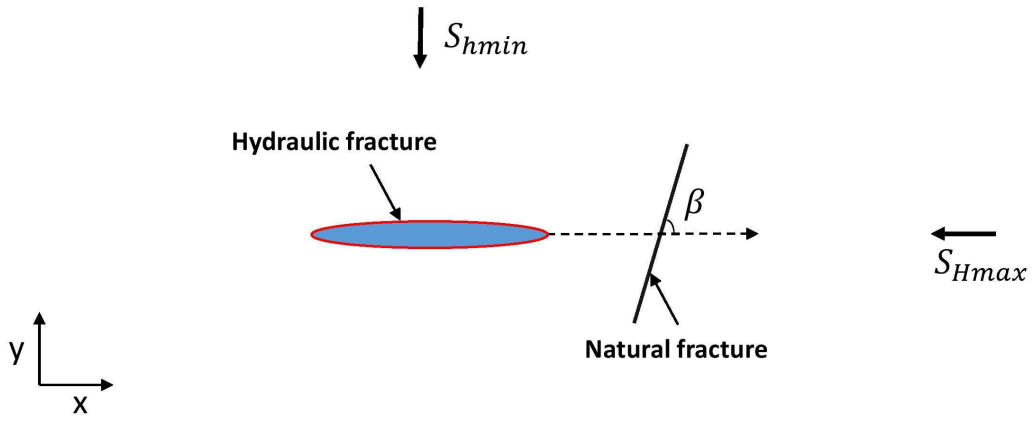

Figure 2.2: Schematic showing a hydraulic fracture approaching a natural fracture.

fractures and divert the hydraulic fracturing propagation when the product of fracturing fluid flow rate, Q, and viscosity, μ, is small (i.e., $Q\mu$ is a small value); otherwise, when the product value is large, hydraulic fractures tend to cross natural fractures and propagate in the same direction, like planar fractures. We considered a slick water for hydraulic fracturing which is of very-low viscosity (0.64 cp), and thus, hydraulic fractures diverted into natural fractures for the four relative angles resulting in a complex fracture geometry (Fig. 2.3). In addition, the TFSA is also affected by the relative angles as shown in Fig. 2.4. When the relative angle is 0°, hydraulic fractures will propagate in the direction of the maximum horizontal stress after diverting into natural fractures (Fig. 2.2). In this case, the compressional stress acting perpendicular to the surface of hydraulic fractures is the minimum horizontal stress. As the relative angle increases, the compressional stress acting on hydraulic fractures after diverting into natural fractures increases. Eventually, at 90° the compressional stress acting on hydraulic fractures is the maximum horizontal stress. In summary, the fracture growth becomes more restricted with relative angle (Fig. 2.3). Therefore, as can be seen from Fig. 2.4, a smaller relative angle generates a higher TFSA.

2.3.1.2 Effect of natural fracture length on TFSA

As observed from the data obtained from Barnett shale [42], the length of natural fractures in naturally fractured reservoirs is not constant. Generally, natural fractures with different lengths

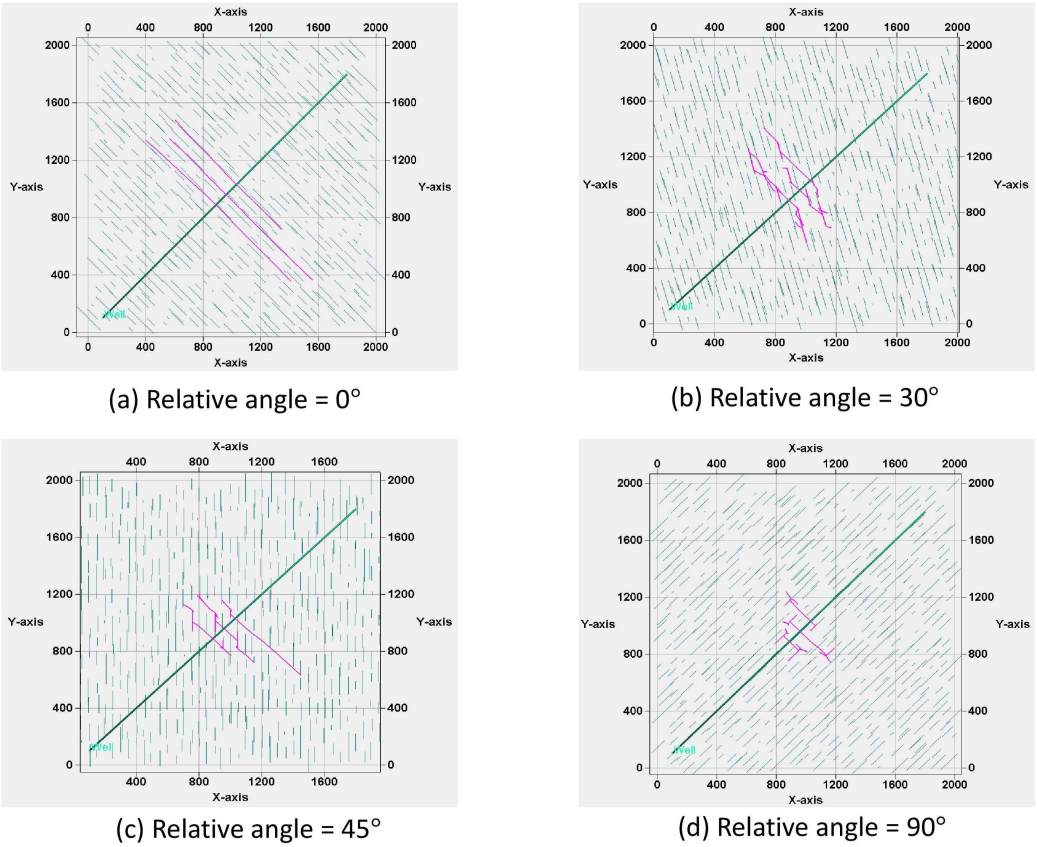

Figure 2.3: Fracture network at the end of hydraulic fracturing operation for four different relative angles between hydraulic fractures and natural fractures.

are generated using a normal distribution to replicate the field case. In this sensitivity analysis, we considered two different distributions of natural fracture length as given in Table 2.3 with a fixed relative angle of 45°. All other parameters were used as described in Table 2.1. The 2D trace of natural fracture network and final complex fracture network obtained at the end of hydraulic fracturing operation for these two cases are shown in Fig. 2.5.

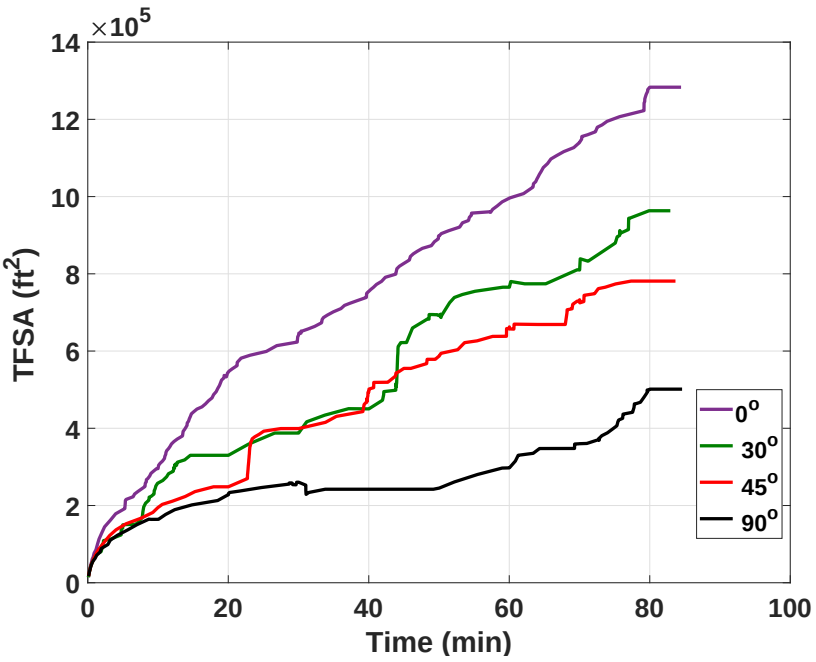

Figure 2.4: Comparison of TFSA for four different relative angles between hydraulic fractures and natural fractures.

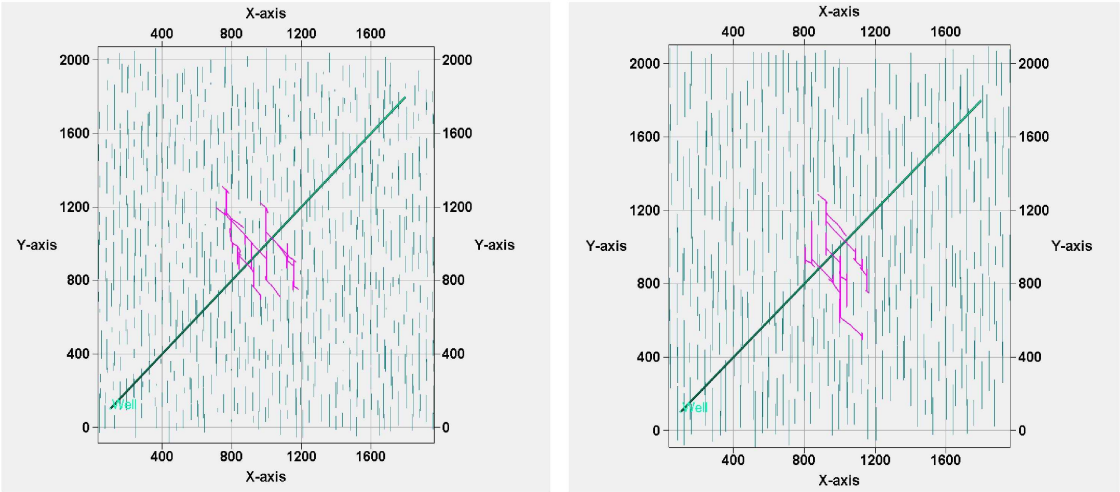

(a) Average length = 100 ft

(b) Average length = 200 ft

Figure 2.5: Fracture network at the end of hydraulic fracturing operation for two different natural fracture length distributions.

It is observed that the hydraulic fracture propagation pattern depends on the length of natural fractures. Hydraulic fractures tend to propagate in the direction of natural fractures when the length of natural fractures is long; whereas in the case of short natural fracture length, they tend to propagate in the original hydraulic fracture propagation direction. In addition, TFSA is also affected by natural fractures length, as shown in Fig. 2.6.

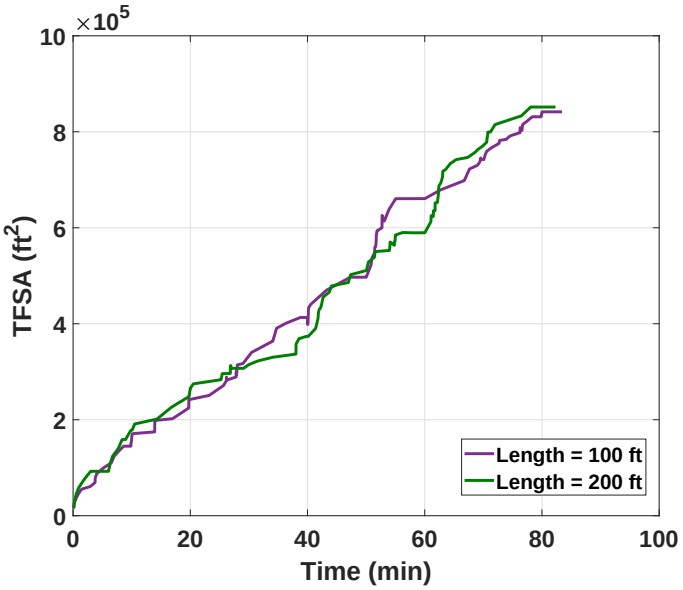

Figure 2.6: Comparison of TFSA for two different natural fracture length distributions.

Until a hydraulic fracture diverts into a natural fracture, the compressional stress acting perpendicular to the fracture surface area is the minimum horizontal stress. However, after it diverts, the compressional stress becomes greater than the minimum horizontal stress. This happens due to a change in the fracture orientation until the fracture grows out of a natural fracture. For longer natural fracture lengths, the high compressional strength will act for a longer time period which further restricts fracture growth and generates a less TFSA compared to those of shorter natural fracture lengths.

	Relative angle	Spacing (ft)	Friction coefficient	Length (ft)	
Average	45°	40	0.6	100	200
Standard deviation	0°	5	0	50	50

Table 2.3: Natural fracture distribution with different lengths.

2.3.1.3 Effect of natural fracture spacing on TFSA

In this sensitivity analysis, we considered two different distributions for natural fracture spacing as given in Table 2.4 with a fixed relative angle of 45°. All other parameters were kept as described in Table 2.1. The 2D trace of natural fracture network and final complex fracture network obtained at the end of hydraulic fracturing operation for these two cases are shown in Fig. 2.7.

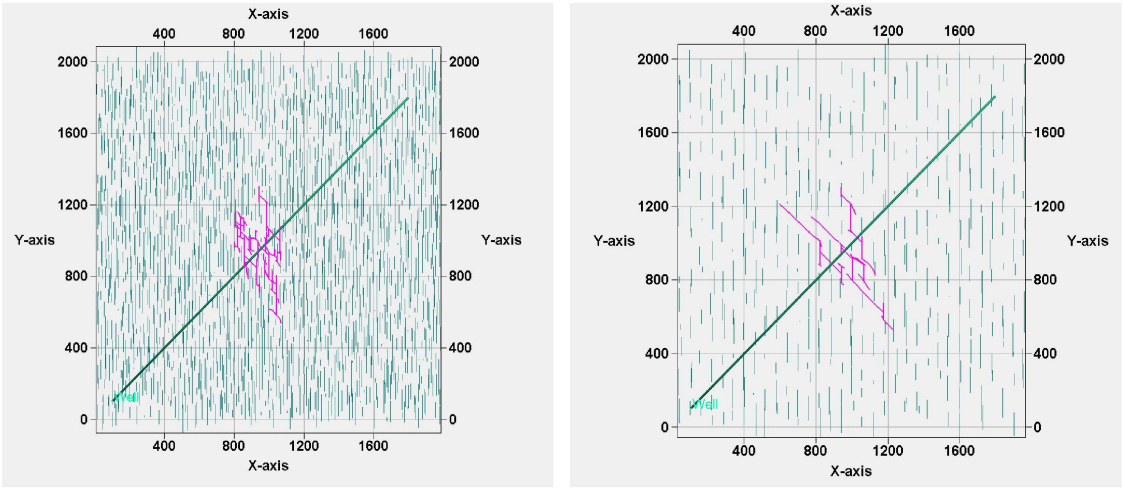

(a) Spacing= 20 ft (b) Spacing = 60 ft

Figure 2.7: Fracture network at the end of hydraulic fracturing operation for two different natural fracture spacing distributions.

It is observed that a decrease in natural fracture spacing leads to a more complex fracture geometry, as more natural fractures are likely to be encountered by hydraulic fractures. Because of this complex interaction of hydraulic fractures with multiple closely-spaced natural fractures,

TFSA decreases with natural fracturing spacing as shown in Fig. 2.8.

	Relative angle	Length (ft)	Friction coefficient	Spacing (ft)	
Average	45°	100	0.6	20	60
Standard deviation	0°	50	0	5	5

Table 2.4: Natural fracture distribution with different spacing values.

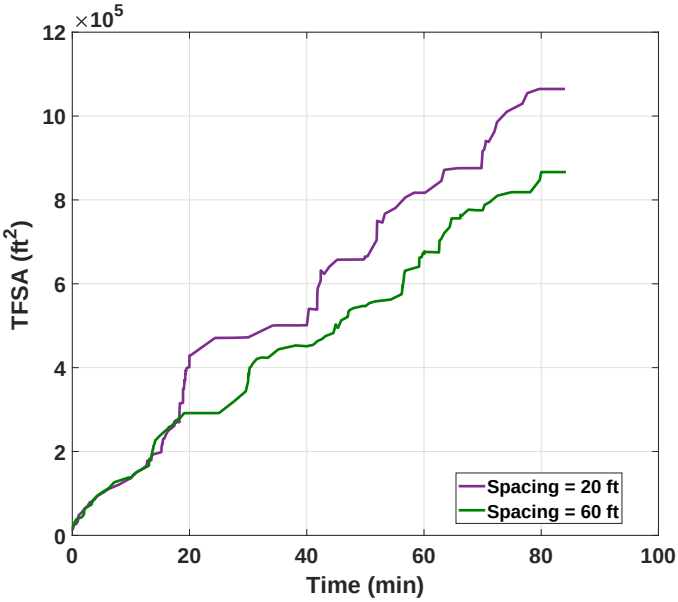

Figure 2.8: Comparison of TFSA for two different natural fracture spacing distributions.

Based on the sensitivity analysis presented above, we can observe that natural fracture attributes (e.g., spacing, length and orientation) have a major impact on complex fracture growth during hydraulic fracturing in naturally fractured unconventional reservoirs. Therefore, it is very important to consider the interaction between hydraulic fractures and natural fractures to optimize the hydraulic fracturing treatment in naturally fractured unconventional reservoirs. In practice, microseismic measurements can be used to partially predict the distribution of natural fractures by comparing the effective stimulated volume for a given distribution of natural fractures. In this

work, we assume that the natural fracture distribution is available, which is used as a feedback to design a model-based feedback control framework to compute the pumping schedule by maximizing the TFSA for given fracturing resources.

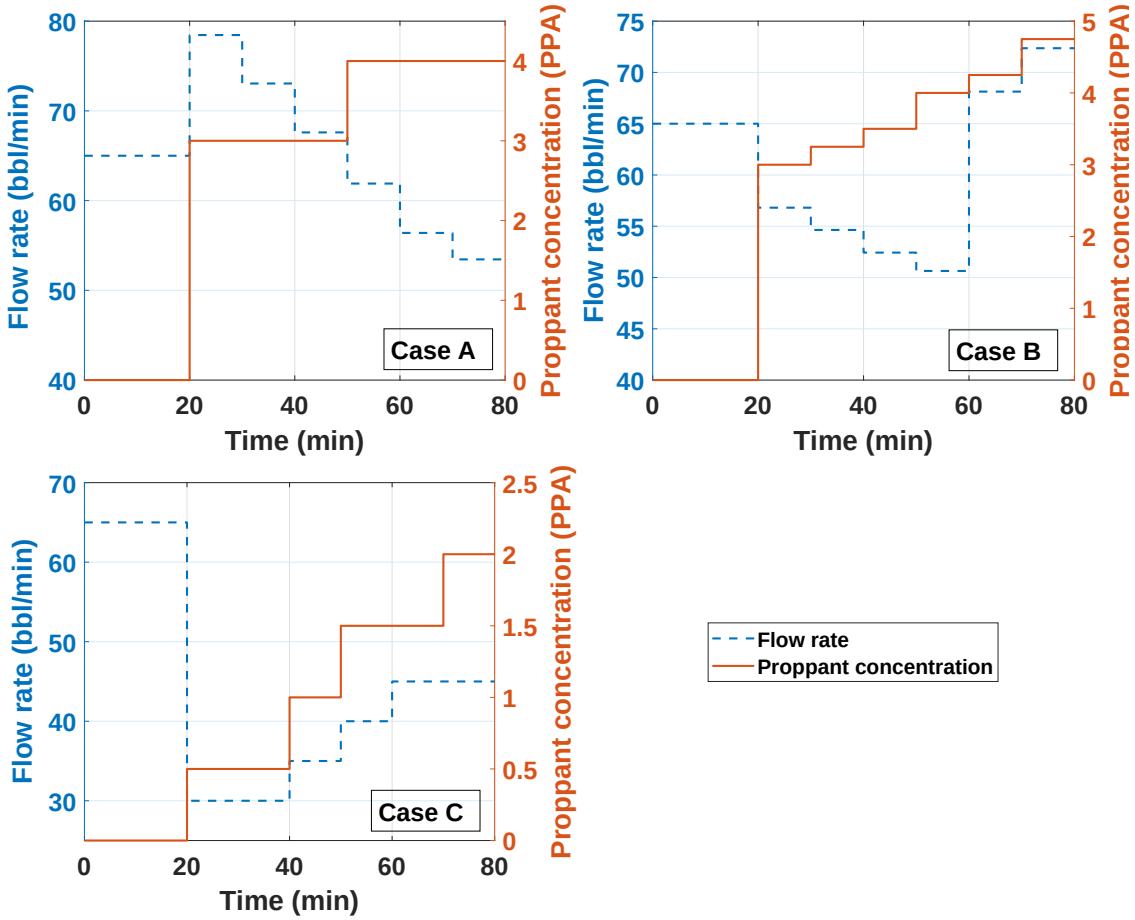

Figure 2.9: Pumping Schedules used for sensitivity analysis.

2.3.2 Effect of pumping schedule on TFSA

In this subsection, we performed a sensitivity analysis to find the effect of fracturing fluid pumping schedule (i.e., flow rate and proppant concentration at the wellbore) on the TFSA at the end of pumping for given rock properties (e.g., Young's modulus, Poisson ratio and in-situ stresses),

natural fracture distribution (length, orientation and spacing between natural fractures) and amount of proppant. The statistical parameters used to generate the natural fracture distribution are given in Table 2.7. We considered a total amount of $M_{prop} = 487200$ lb proppant to be injected for creating fractures in a stage. All the other parameters used in the simulations are given in Table 2.1. We generated three fractures in a single stage with a fixed fracture spacing. For the purpose of sensitivity studies, we considered three cases with three different pumping schedules. The pumping schedule used in each case and the evolution of TFSA with time are shown in Fig. 2.9 and Fig. 2.10, respectively. We can clearly see that the TFSA depends on pumping schedules.

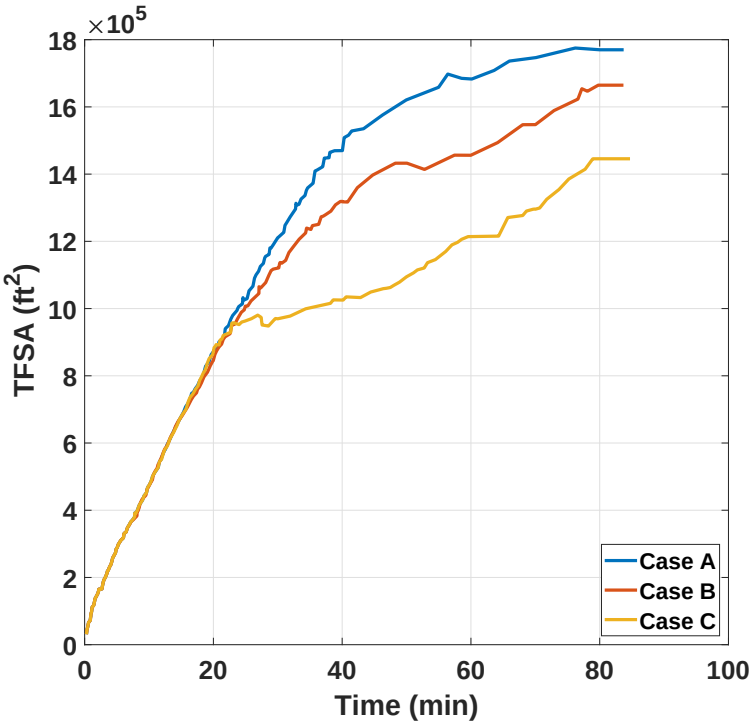

Figure 2.10: Comparison of TFSA for three cases with different pumping schedules.

Parameters	Value
Reservoir rock type	Consolidated sandstone
Permeability	$0.0001 - 0.0005$ mD
Porosity	0.08
Reservoir pressure	5000 psi
Unpropped fracture conductivity	10^{-3} mD.ft
Production time	30 years

Table 2.5: Reservoir properties used for the oil production simulation.

Thereafter, we simulated the corresponding oil production for 30 years in each case using the reservoir properties given in Table 2.5 and the generated complex fracture geometry at the end of hydraulic fracturing operation. The cumulative oil production is shown in Fig. 2.11, where it can be observed that the oil production rate is proportional to the TFSA at the end of pumping. This can also be seen from the results presented in Table 2.6, where it is observed that a reduction of 18% in the TFSA at the end of pumping leads to a reduction of around 60% in the cumulative oil production at the end of 30 years. This is mainly due to the fact that the drainage area for hydrocarbon recovery is directly related to TFSA, and achieving a greater TFSA will lead to a greater oil production rate in naturally fractured unconventional reservoirs. Therefore, because of complex fracture growth, the main goal of hydraulic fracturing in naturally fractured unconventional reservoirs should be to maximize the TFSA by manipulating the fracturing fluid pumping schedule for given resources as it will lead to more oil recovery.

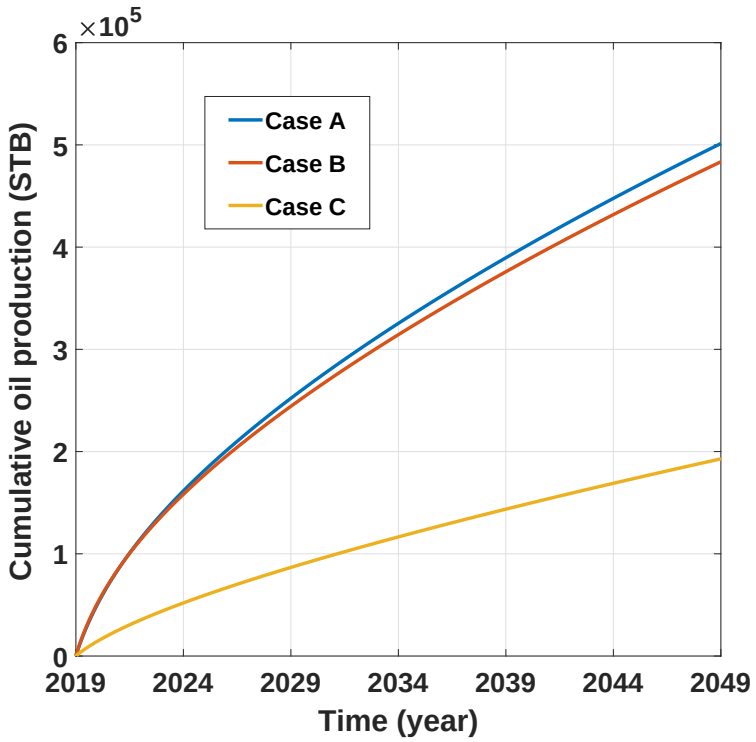

Figure 2.11: Cumulative oil production over time for three cases with different pumping schedules.

2.4 Background on pumping schedule design techniques

In this section, we present currently available pumping schedule design techniques. Nolte [43] developed a power-law type proppant concentration schedule, $C_0(t)$, which is given below:

$$C_0(t) = \begin{cases} C_{target}\left(\frac{t-t_p}{t_e-t_p}\right)^{\epsilon} & \text{for } t \geq t_p \\ 0 & \text{for } t < t_p \end{cases} \tag{2.10}$$

where the desired proppant concentration at the end of hydraulic fracturing operation is denoted using C_{target}, ϵ is an exponent which depends on fracturing fluid efficiency η, the total time for pumping is denoted using t_e, and $t_p = \epsilon t_e$ is the pad time at which injection of proppant is started. Because of its easy-to-implement nature, Nolte's pumping schedule has been widely used, however it has the following practical limitations: (1) both proppant settling due to gravity and practical constraints are not considered; (2) because of the predefined form if there is a plant-model mismatch, it

Case	TFSA (ft^2)	% Change in TFSA compared to case A	Cumulative oil production (STB)	% Change in production compared to case A
Case A	1769942	0	501542	0
Case B	1664617	- 5.9	483678	- 3.6
Case C	1445647	- 18.3	192969	- 61.5

Table 2.6: TFSA and cumulative oil production for three cases with different pumping schedules.

will lead to early termination of hydraulic fracturing by creating a shorter propped fracture length; (3) the pumping schedule is designed offline and applied in an open-loop manner to a hydraulic fracturing process; (4) focused only on a single hydraulic fracture; and (5) interaction between hydraulic fractures and natural fractures is not considered.

Recently, to overcome the limitations of Nolte's pumping schedule, a new model-based control system was developed to compute fracturing fluid pumping schedules online to achieve a uniform proppant distribution and optimal fracture geometry in simultaneously growing multiple fractures [1]. Specifically, they considered a dynamic model of simultaneously propagating multiple fractures including fracture propagation, stress shadow effect and proppant transport. However, they did not consider the interaction between hydraulic fractures and natural fractures, which resulted in fractures with a planar shape.

As shown from the sensitivity analysis presented in Section 2.3, hydraulic fracturing operation in naturally fractured unconventional reservoirs may result in a complex fracture geometry and it is very important to maximize the TFSA at the end of pumping as it is directly related to oil production rate. Pumping schedule design techniques mentioned above, which were developed to achieve a specific fracture geometry (length, width and height), may not result in the maximum TFSA when directly applied to naturally fractured unconventional reservoirs. Therefore, in the following section, a model predictive controller (MPC) is developed to compute a pumping schedule that will maximize the TFSA in naturally fractured unconventional reservoirs by utilizing Mangrove, which will eventually lead to an enhanced oil production rate.

2.5 Handling computational requirement in control of hydraulic fracturing processes

The UFM described using Eqs. (2.1)–(2.8) is computationally very expensive to be used directly for the design of MPC. In this work, we developed a ROM using MOESP algorithm to describe hydraulic fracture propagation and proppant transport phenomena in naturally fractured unconventional reservoirs, which is given below:

$$x(t_{k+1}) = Ax(t_k) + Bu(t_k) \tag{2.11a}$$

$$y(t_k) = Cx(t_k) \tag{2.11b}$$

where $u(t_k) = [Q_{x0}(t_k), C_0(t_k)]^{\mathrm{T}}$ are the input variables, $Q_{x0}(t_k)$ and $C_0(t_k)$ are the fracturing fluid flow rate and proppant concentration injected at the wellbore, respectively, the output variable, $y(t_k) = [A_{frac}(t_k)]$ is the TFSA, and the ROM states are represented using $x(t_k)$. For a system with a given order, the model parameters to be determined include the matrices A, B, and C, and the initial state estimate, $x(0)$, using a training data set.

For training, we used an open-loop simulation data obtained using Mangrove to obtain a 3^{rd} order linear time-invariant state-space model. The training input is chosen by considering the minimum and maximum allowable fracturing flow rate and proppant concentration. Fig. 2.12 shows the comparison between the estimated and true TFSA with time. It is observed that the estimated TFSA from the ROM quickly converges to the true value obtained from the high-fidelity process model. The computational requirement to solve Eq. (2.11) is a small fraction relative to that of solving the UFM, Eqs. (2.1)–(2.8). We have validated the ROM by comparing its performance with the high fidelity model by considering a different pumping schedule within the limits of minimum and maximum fracturing flow rate and proppant concentration considered while developing ROM. Fig. 2.13 shows that TFSA obtained from the ROM is close to the high fidelity model.

In the present work, we assumed that TFSA is measurable, which is then used for estimation of

the ROM states at time $t = t_k$, $x(t_k)$, using a Kalman filter, which is given in the following form:

$$\hat{x}(t_{k+1}) = A\hat{x}(t_k) + Bu(t_k) + M(t_k)(y_m(t_k) - \hat{y}(t_k)) \tag{2.12a}$$

$$M(t_k) = P(t_k)C^T(R(t_k) + CP(t_k)C^T)^{-1} \tag{2.12b}$$

$$P(t_{k+1}) = (I - M(t_k)C)P(t_k) \tag{2.12c}$$

where the variables estimated by the Kalman filter are denoted using $\hat{(\cdot)}$, $y_m(t_k) = [A_{frac}(t_k)]$ is the TFSA, the process and measurement noise covariance matrices are denoted using Q and R, respectively, $M(t_k)$ is the gain of Kalman filter, and $P(t_k)$ denotes the state estimation error covariance. In this work, a Kalman filter is used for state estimation. However, other state estimators such as Luenberger observer or moving horizon estimator can be readily used.

Remark 2. *In this work, Kalman filter is used to estimate the ROM states which will also handle any plant-model mismatch by considering the real-time measurement of TFSA. Furthermore, due to the nature of closed-loop operation based on the proposed controller design technique, model-plant mismatch would be handled.*

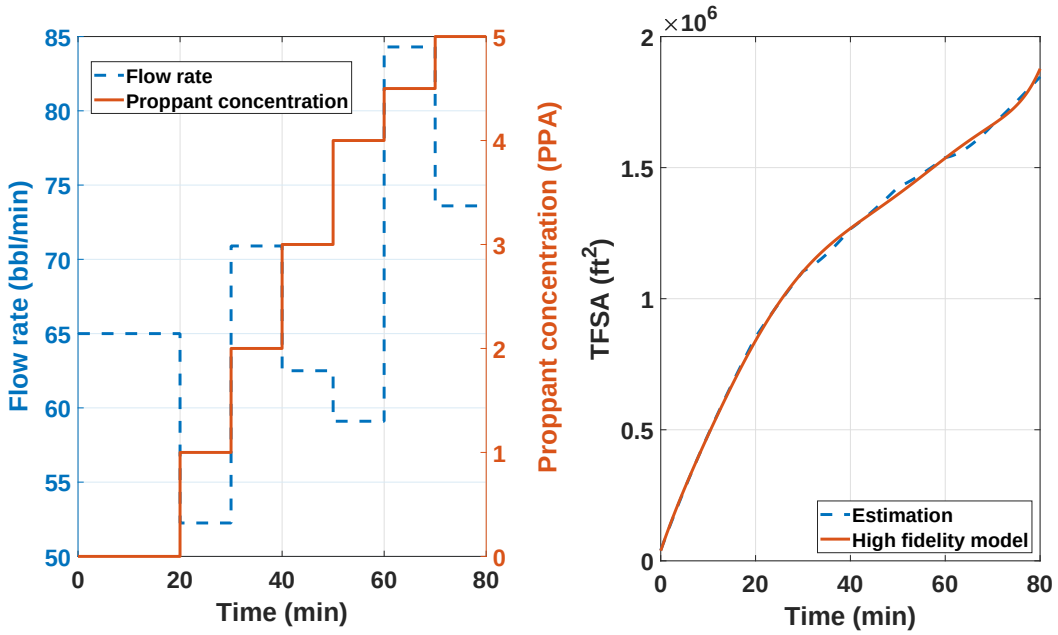

Figure 2.12: Comparison between the true values and the estimates of TFSA for a given pumping schedule.

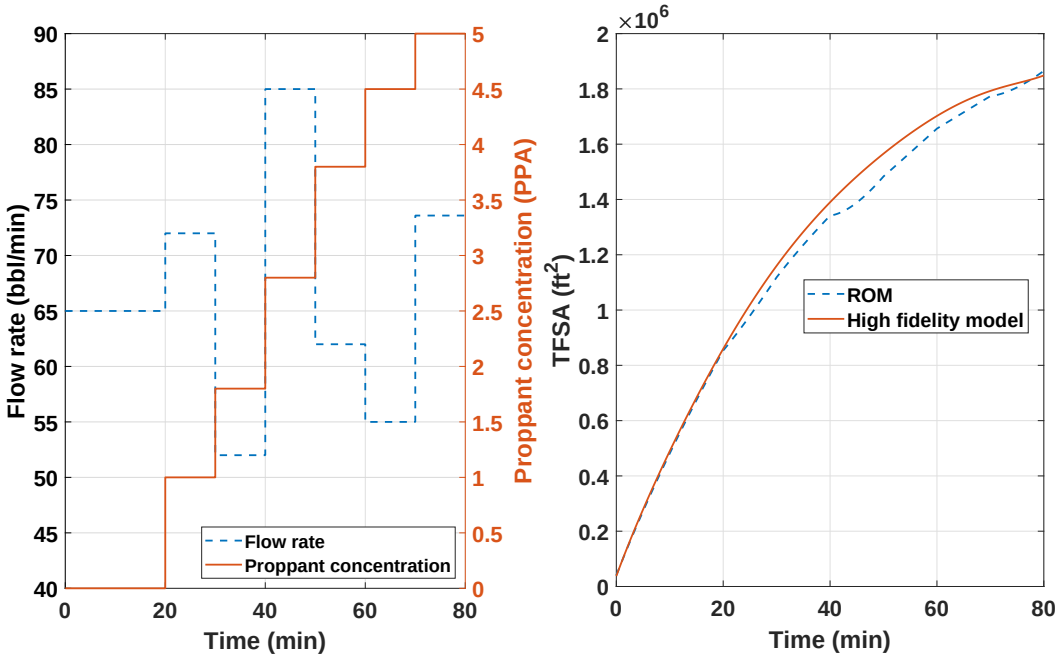

Figure 2.13: Validation of ROM by comparing it with high fidelity model for a given pumping schedule.

Remark 3. *Please note that it is not practical to measure TFSA in real-time. However, TFSA can be estimated from other available measurements using state estimators such as Kalman filter or moving horizon estimator. In practice, we have very limited access to real-time measurements such as the fracture width at the wellbore. Real-time measurement of fracture width at the wellbore can be obtained using the wellbore pressure data and the elasticity equation relating the fracture width at the wellbore and the wellbore pressure [24, 44, 45, 46, 47, 48]. Previously, we have used this available measurement to estimate unmeasurable variables such as proppant concentration across the fracture and average fracture width using a Kalman filter [23, 29, 30]. Similarly, we can estimate TFSA by using a Kalman filter and the available real-time measurement of fracture width at the wellbore.*

2.6 Model-based feedback control system for enhancing TFSA in naturally fractured unconventional reservoirs

This section presents a MPC formulation to compute an optimal pumping schedule that maximizes the TFSA in naturally fractured unconventional reservoirs at the end of hydraulic fracturing process. The following MPC optimization problem is solved utilizing the ROM and Kalman filter to compute the optimal pumping schedule:

$$\max_{\substack{C_{stage,k},\ldots,C_{stage,8}\\ Q_{stage,k},\ldots,Q_{stage,8}}} \quad A_{frac}(t_f) \tag{2.13a}$$

$$\text{s.t.} \quad y_m(t_k) = A_{frac}(t_k) \tag{2.13b}$$

$$\text{ROM, Eq. (2.11)} \tag{2.13c}$$

$$\text{Kalman filter, Eq. (2.12)} \tag{2.13d}$$

$$C_{stage,k-1+m} \leq C_{stage,k+m} \leq 5 \text{ PPA} \tag{2.13e}$$

$$Q_{min} \leq Q_{stage,k+m} \leq Q_{max} \tag{2.13f}$$

$$m = 1, \ldots, 8-k \tag{2.13g}$$

$$\Delta \left(\sum_{k=1}^{8} Q_{stage,k} C_{stage,k} \right) = M_{prop} \tag{2.13h}$$

where the duration of each sampling is given by Δ, t_k is the time of k^{th} sample, $y_m(t_k)$ is the TFSA measured at $t = t_k$, t_f is the hydraulic fracturing total operation time, and the manipulated input variables, $C_{stage,k}$ and $Q_{stage,k}$, are obtained by solving Eq. (2.13) with a shrinking prediction horizon $N_p = t_f - t_k$.

In the optimization problem of Eq. (2.13), a Kalman filter, Eq. (2.13d), is used to estimate unmeasurable ROM states and it is initialized at every sampling time utilizing the TFSA measured in real-time, which is described by Eq. (2.13b). Eqs. (2.13e)-(2.13f) are the constraints on the manipulated input variables (e.g., proppant concentration and fracturing fluid flow rate injected at the wellbore). The units of fracturing fluid flow rate and proppant concentration are bbl/min and PPA (1 pound of the proppant added to one gallon of fracturing fluid), respectively. The total amount of proppant injected is constrained using Eq. (2.13h).

2.7 Closed-loop simulation results under the proposed MPC

In this section, we present the closed-loop simulation results to signify the performance of our proposed MPC scheme. For all the cases, we considered a single stage hydraulic fracturing oper-

ation to generate three simultaneously propagating multiple fractures for a given natural fracture distribution. The statistical parameters used to generate the natural fracture distribution are given in Table 2.7 and the generated natural fracture distribution is shown in Fig. 2.14. The total proppant amount considered is $M_{prop} = 487200$ lb. All the other parameters used in the simulations are given in Table 2.1. The high fidelity model of Mangrove described in Section 2.2 was utilized to simulate a hydraulic fracturing operation in naturally fractured unconventional reservoirs. This model is initially used with a given training input for generating the input/output data which was used to develop a ROM of the process. We then designed a Kalman filter for state estimation using this ROM, which eventually helped us in developing the complete MPC scheme. The Kalman filter and the proposed MPC were initialized at the beginning of hydraulic fracturing operation. In the proposed MPC, Δ and t_f values were chosen to be 10 min and 80 min, respectively. This implies that the fracturing fluid pumping schedule consists of 8 stages, each with a duration of 10 min. We assumed that the measurement of TFSA, $A_{frac}(t_k)$, was available at the beginning of each pumping stage (Eq. (2.13b)). The unmeasurable ROM states were then predicted with the help of real-time measurement via the Kalman filter. Using these estimated states, the proposed MPC computed the control input over a prediction horizon length of N_p to maximize the TFSA at the end of hydraulic fracturing operation, which will lead to an enhanced oil production rate due to a higher drainage area available for hydrocarbon recovery. We applied the first step of solution, $C_{stage,k}$ & $Q_{stage,k}$, to the high-fidelity model of Mangrove in a sample-and-hold fashion and this procedure was repeated at every sampling time until the end of the process.

	Length (ft)	Spacing (ft)	Orientation	Friction coefficient
Average	500	100	15	0.5
Standard deviation	250	50	15	0

Table 2.7: Natural fracture distribution used in the closed-loop simulation.

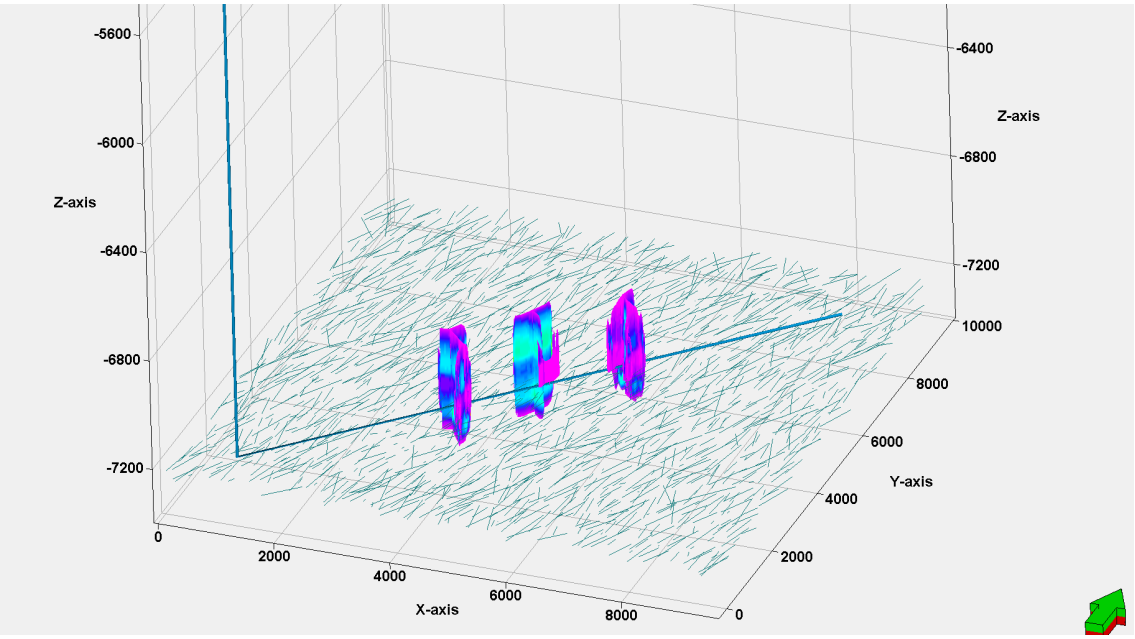

Figure 2.14: Fracture geometry at the end of hydraulic fracturing operation under the proposed MPC.

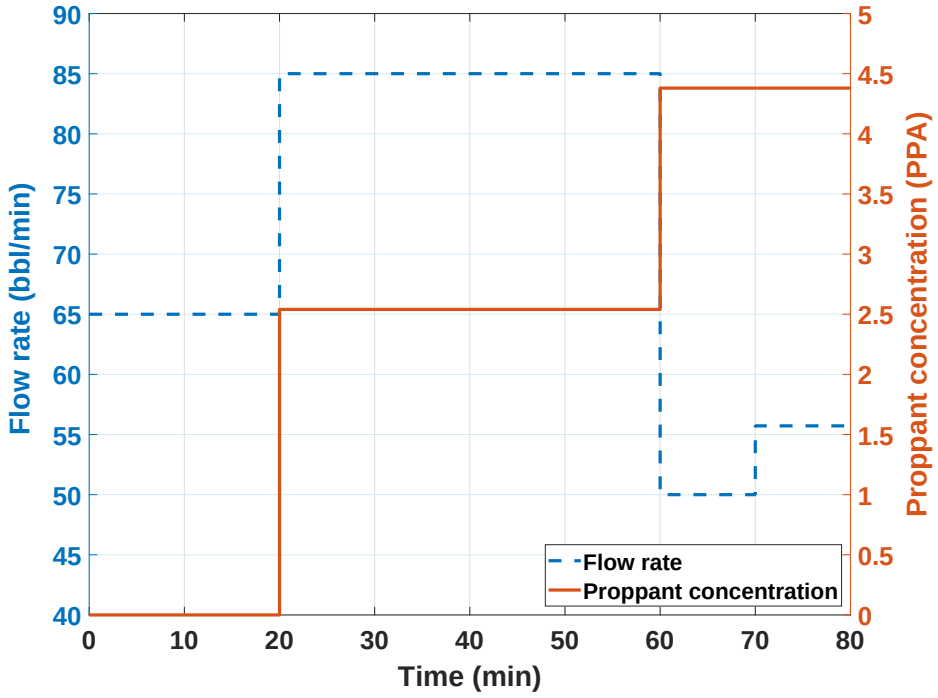

Figure 2.15: Pumping schedule obtained under the proposed MPC.

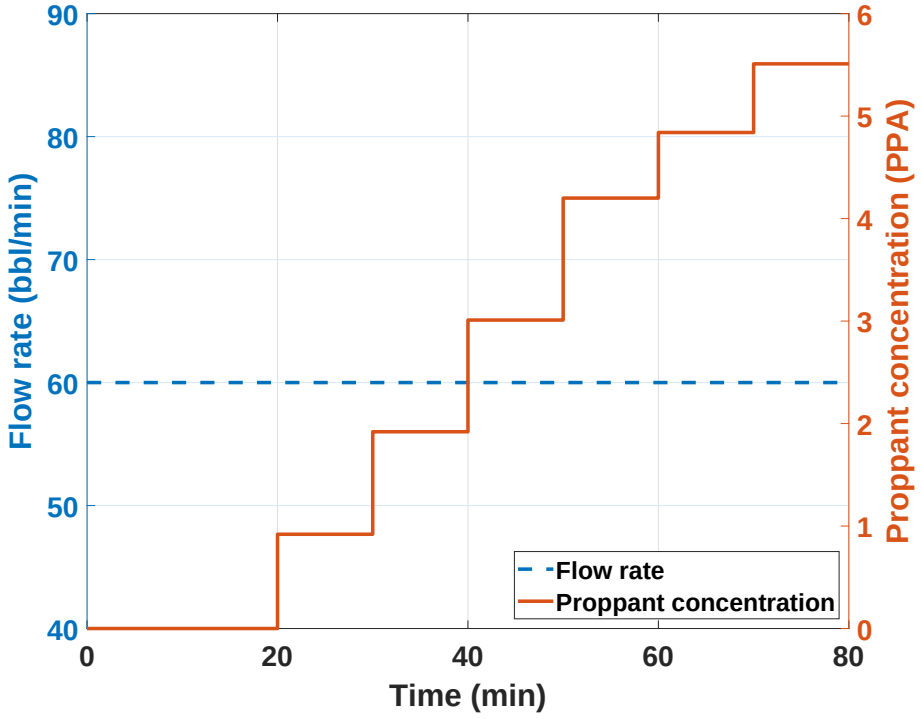

Figure 2.16: Nolte's pumping schedule with input constraints being considered.

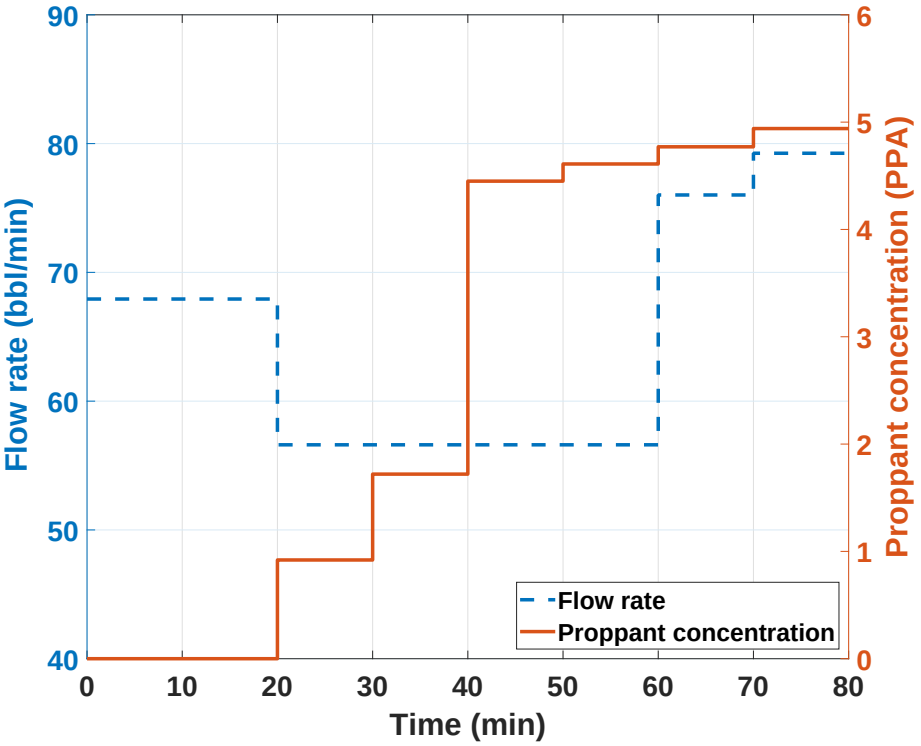

Figure 2.17: Pumping schedule obtained by the method proposed by Siddhamshetty et al. [1].

The pumping schedule obtained under the proposed MPC scheme (Fig. 2.15) is then fed as an input to Mangrove. The obtained fracture geometry at the end of hydraulic fracturing operation under the proposed MPC is presented in Fig. 2.14. For given rock properties and natural fracture distributions, hydraulic fractures divert into natural fractures resulting in a complex fracture geometry. We then compared the performance of the pumping schedule computed by the proposed MPC with existing pumping schedules such as Nolte (Fig. 2.16) and the one introduced by Siddhamshetty et al. [1] (Fig.2.17), which were developed without considering natural fractures. All the other parameters such as Young's modulus, Poisson ratio, and proppant amount are kept same in all the cases. Fig. 2.18 compares the evolution of the TFSA for the three cases. Fig. 2.19 and Fig. 2.20 show the comparison of the cumulative oil production and oil production rates for the three cases. We can see clearly from the figures that the pumping schedule under the proposed MPC maximizes the TFSA, which subsequently leads to the maximum oil production rate and maximum cumulative oil production compared to other pumping schedules.

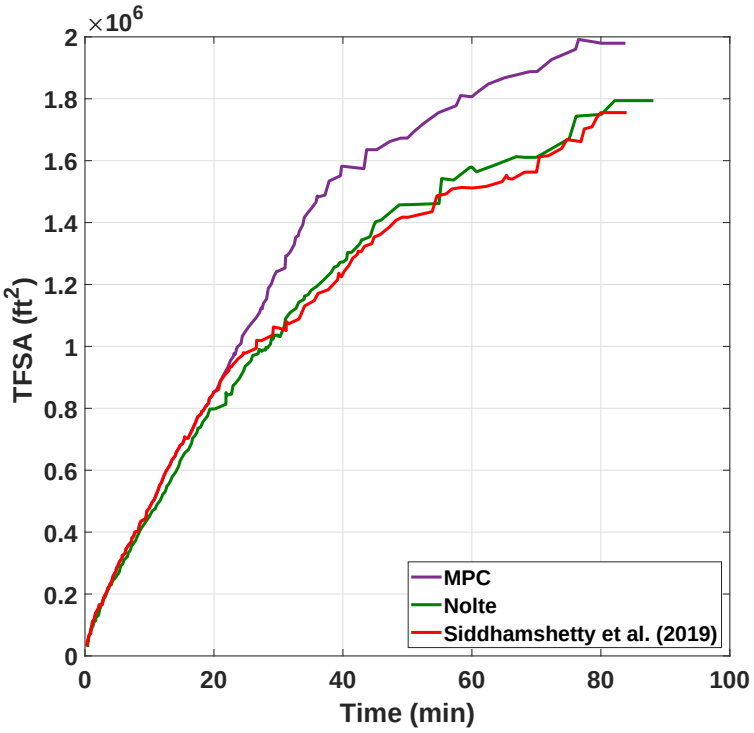

Figure 2.18: Comparison of TFSA under the proposed MPC, Nolte's and Siddhamshetty et al. [1] pumping schedules.

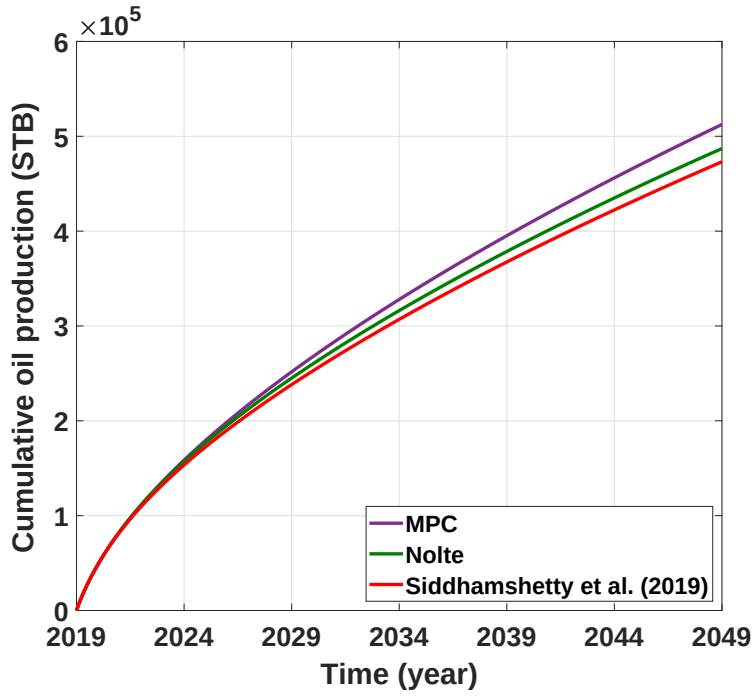

Figure 2.19: Comparison of cumulative oil production under the proposed MPC, Nolte's and Siddhamshetty et al. [1] pumping schedules.

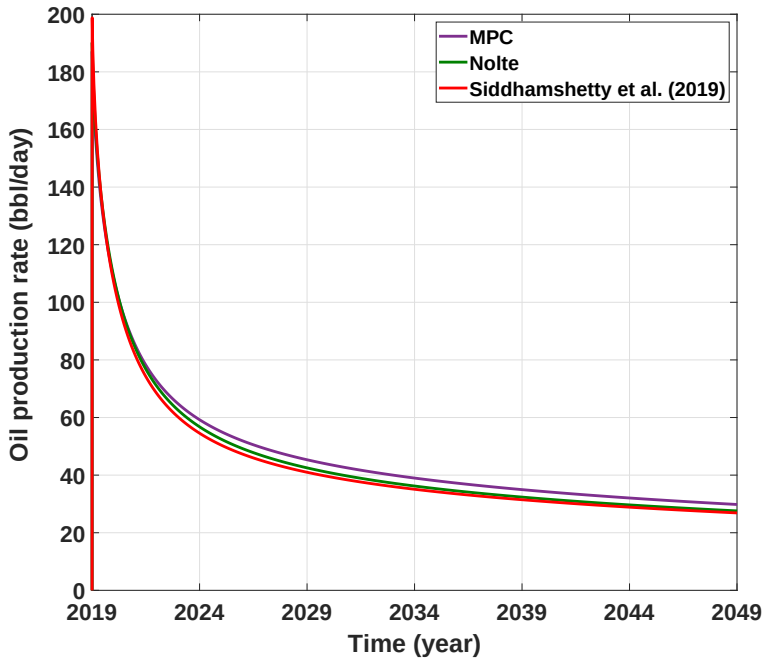

Figure 2.20: Comparison of oil production rates under the proposed MPC, Nolte's and Siddhamshetty et al. [1] pumping schedules.

We reported the NPV of oil produced for these three cases in Table 2.8. Using the proposed MPC will result in an revenue that is \$0.74 millions and \$0.4 millions more than those obtained by Siddhamshetty et al. [1] and Nolte [43], respectively.

	TFSA (ft^2)	Cumulative oil production (STB)	NPV (M\$)
MPC	1979450	512707	13.36
Nolte	1793945	487310	12.96
Siddhamshetty et al. [1]	1755249	473338	12.62

Table 2.8: TFSA, cumulative oil production and NPV of oil produced under the proposed MPC, Nolte's and Siddhamshetty et al. [1] pumping schedules.

Because linear ROMs were used to solve this problem, we achieved a significant reduction in the computational requirement. The time required to solve the optimization problem, Eq. (2.13), at every sampling time instant is given in Table 2.9. Since the problem was solved using a shrinking horizon approach, we can see that the computational time with every iteration has a tendency to decrease. Please note that all calculations were performed using MATLAB on a Dell workstation, powered by Intel(R) Core(TM) i7-4790 CPU@3.60GHz, running the Windows 8 operating system.

Pumping stage number	Computational time (s)
1	4.93
2	0.70
3	0.56
4	0.36
5	0.30
6	0.14
7	0.19
8	0.05

Table 2.9: Computational time required to solve the optimization problem, Eq. (2.13), at each pumping stage.

Natural fractures are present in most of unconventional reservoirs and affect hydraulic fracture propagation. Therefore, we cannot ignore the interaction of hydraulic fractures with natural fractures when we design pumping schedules to inject given fracturing resources. We have to utilize these interaction to achieve an even greater TFSA, which would not have been possible to achieve without considering natural fractures. Drainage area for hydrocarbon recovery is directly related to TFSA. Therefore, achieving a greater TFSA will lead to an increased oil production rate in naturally fractured unconventional reservoirs. The model-based pumping schedule design technique developed in this work considers the interaction of hydraulic fractures with natural fractures. Therefore, we were able to achieve a TFSA greater than those of the existing pumping schedules which were developed without considering natural fractures.

3. NUMERICAL STUDY OF THE EFFECT OF PSA AND FC ON SHALE GAS PRODUCTION: APPLICATION FOR MULTI-SIZE PROPPANT PUMPING SCHEDULE DESIGN

3.1 Introduction

In the hydraulic fracturing operation for unconventional reservoirs, it is important to achieve an optimal fracture geometry to maximize the gas production [23]. Lately, researchers have developed model-based feedback control strategies to achieve an optimal fracture geometry [1, 23, 24, 25, 26, 27, 28, 29, 30, 31, 32, 49, 50]. However, they used a single-size proppant to design pumping schedules.

For determining the oil and gas production from unconventional reservoirs, average propped surface area (PSA) and average fracture conductivity (FC) of the propped hydraulic fractures play an important role. Average PSA and average FC depend largely on the injected proppant diameter. Existing studies on average PSA or average FC considered these two effects separately, and did not consider their combined effect on shale gas production. Wahl [51] discussed, for the first time, the importance of effective total fracture surface area (TFSA), instead of TFSA, for horizontal fractures, and developed a new technique to maximize the effective TFSA. Ramurthy et al. [52] elaborated in detail that different shale plays require different types of treatment, either maximizing surface area or conductivity. They also presented tests like Brinell Hardness (BHN) and Diagnostic Fracture Injection Test (DFIT) to determine the type of treatment required for the sample reservoir being tested. Schmidt et al. [53] have done an extensive study on a laboratory scale to understand the impact of multi-size proppant addition on FC. Recently, various experimental and simulation studies have been conducted to understand the phenomena like transport, embedment, crushing, distribution and settling of the injected proppant [54, 55, 56, 57]. Hu et al. [58] further discussed a multi-size proppant pumping schedule in a pre-existing straight fracture on a laboratory scale. Specifically, their objective was to transport proppant deeper into the fracture,

instead of considering PSA or FC to quantify shale gas production from unconventional reservoirs. Although researchers have modeled shale gas flow using microseismic data [59] and predicted horizontal well productivity in gas condensate reservoirs [60], it is worthwhile to note that none of the previous studies considered both the average PSA and average FC for multiple simultaneously propagating fractures as a quantitative measure to predict shale gas production. Motivated by these considerations, in this chapter, we develop a framework called Sequentially Interlinked Modeling Structure (SIMS) to relate average PSA, average FC, and cumulative shale gas production volume from an unconventional reservoir, when a multi-size proppant pumping schedule is introduced to simultaneously propagating multiple fractures. We further integrate the SIMS framework to obtain a multi-size proppant pumping schedule that maximizes the cumulative shale gas production volume in unconventional reservoirs.

This chapter is structured as follows: In Section 3.2, the use of Petrel as a high-fidelity model to simulate simultaneously propagating multiple fractures is described. In Section 3.3, the effect of changing proppant sizes during the hydraulic fracturing process is presented. In Section 3.4, we present an overview of SIMS, the novel framework proposed in this work. In Section 3.4.1, we explain the first model in detail, where Multivariable Output Error State Space (MOESP)-based reduced-order model (ROM) is constructed using the data generated from Mangrove, which describes the correlation between output variables (i.e., average PSA and average FC) and the input variables (i.e., fracturing fluid flow rate, proppant concentration, and the diameter of proppant particles injected at the wellbore). In Section 3.4.2, we explain the second model in detail, where an Artificial Neural Network (ANN) is trained and deployed to predict the post-shut-in average PSA and average FC from the corresponding pre-shut-in values. In Section 3.4.3, we explain the third model in detail, where a map is generated to determine a correlation between the after-shut-in average PSA and average FC to the cumulative shale gas production volume at the end of 10 years. Next, in Section 3.5, we discuss in brief, various pumping schedules present in the literature. In Section 3.6, we propose an optimization problem using the proposed SIMS framework as described in the previous section, with the constraints on fracturing fluid flow rate, proppant con-

centration and proppant sizes available for injection, to obtain pumping schedules that maximize shale gas production from unconventional reservoirs. Finally, in Section 3.7, results showing that the obtained pumping schedule leads to the maximum cumulative shale gas production from an unconventional reservoir, considering simultaneously propagating multiple fractures, are presented. We also compare the obtained pumping schedule with existing pumping schedules and two other cases, where the objective is to either maximize the average PSA or the average FC of a reservoir separately.

3.2 High-fidelity model

The UFM [22] described in Section 2.2 has been used in this chapter as high-fidelity model.

3.3 Sensitivity analysis to understand the effect of varying proppant size during injection

In this section, we present a sensitivity analysis result showing the effect of changing proppant size on average PSA and average FC in simultaneously propagating multiple fractures. For this analysis, we have used 0.0065 inch and 0.04 inch proppant particles.

Two pumping schedules, which have similar pumping flow rates and concentration profiles but different proppant sizes, were considered in this case, as shown in Fig. 3.1.

These pumping schedules were subsequently used in the UFM to simulate simultaneously propagating multiple fractures and subsequent gas production. Specifically, the first pumping schedule uses only a small-diameter proppant (Case 1), whereas the other includes only a large-diameter proppant (Case 2). For Case 1, we found the average PSA and the average FC at the end of the settling process to be 429780.32 ft^2 and 199.71 $\mathrm{mD{\cdot}ft}$, respectively. For Case 2, we found the average PSA and average FC at the end of the settling process to be 241760.67 ft^2 and 17619.81 $\mathrm{mD{\cdot}ft}$, respectively. The cumulative shale gas production volumes at the end of 30 years in these cases are 368997.94 MSCF and 362948.94 MSCF, respectively. Fig. 3.2 and Fig. 3.3 show the post-settling fracture geometry qualitatively. In the figures, the settled proppant banks are in red, and the unpropped hydraulic fractures are in pink. The figures clearly show that in Case 1, the proppant bank is longer and has penetrated deeper into the fracture than Case 2.

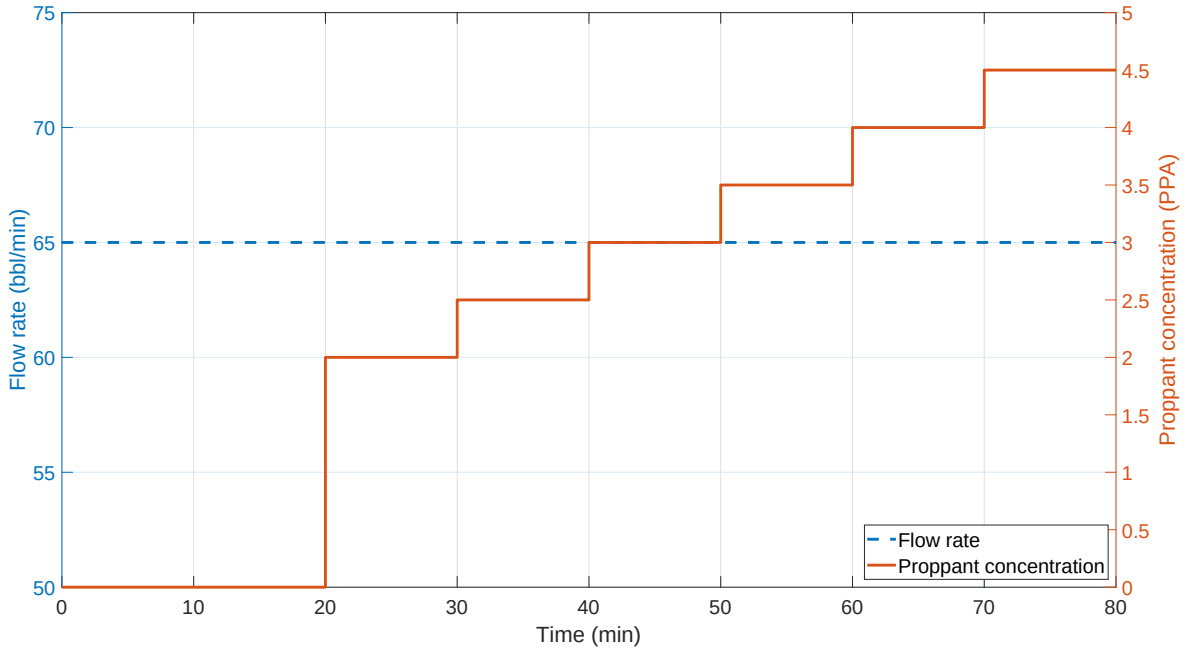

Figure 3.1: Pumping schedule considered in the sensitivity analysis

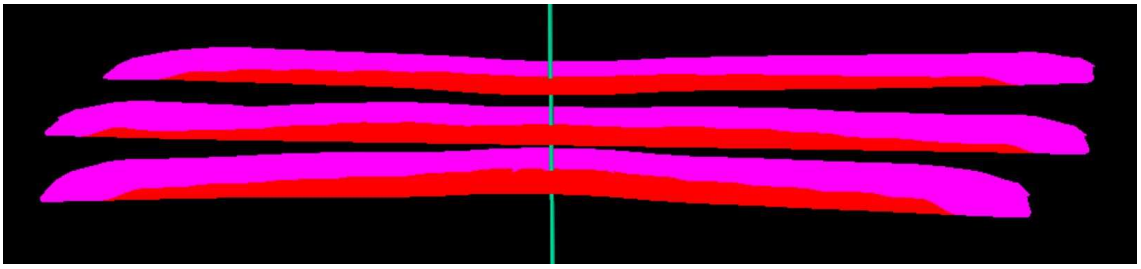

Figure 3.2: Post-settling proppant distribution in Case 1

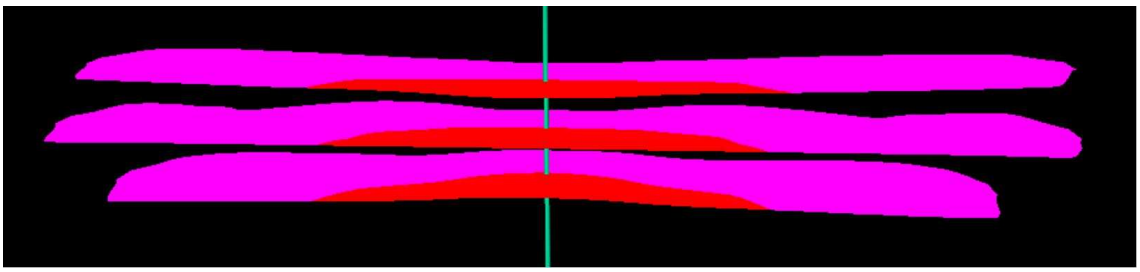

Figure 3.3: Post-settling proppant distribution in Case 2

From the sensitivity analysis, we can conclude a few things: First, average PSA is greater in Case 1 than Case 2. This is primarily because smaller proppant particles tend to suspend in the fracturing fluid for longer times, and hence, can penetrate deeper along the fracture length. Second, average FC in Case 2 is more than Case 1. This is clearly because large proppant particles has high permeability, which directly translates to high average FC of the propped fractures. Third, the cumulative shale gas production volume is almost similar in both the cases. This stems from the fact that we can not rely only on either the average PSA or the average FC separately to accurately predict the shale gas production volume. Instead, there is a dependence of the cumulative gas production volume on both of these parameters, as is visible from the sensitivity analysis.

Motivated by this observation, we propose a new framework in the following section to determine the cumulative shale gas production volume for a given pumping schedule. Then, the proposed model will be further used to obtain pumping schedules to maximize the cumulative shale gas production volume from unconventional reservoirs.

3.4 Proposed SIMS framework

In this chapter, a framework called SIMS is proposed to describe the cumulative shale gas production volume from simultaneously propagating multiple fractures. This approach has two major advantages, as compared to a model that directly correlates the cumulative shale gas production volume from pumping schedules. First, it provides more insight into the process of hydraulic fracturing by breaking it down into smaller parts. An integrated framework having multiple models is easier to comprehend than a single model capturing the fracture propagation, proppant settling and gas production dynamics for an unconventional reservoir. Second, this approach also provides us with average PSA and average FC in the intermediate step after the hydraulic fracturing operation that typically takes a few hours. These parameters are usually of practical importance to the oil and gas industries, instead of just the cumulative shale gas production volume at the end of 10 years.

In this work, we have incorporated three models into the proposed SIMS framework. The first model is an MOESP-based ROM of the fracturing process. The second model is a ANN that has been used to accurately simulate the gravity-induced proppant settling process. The third

model is a map that links the average PSA and the average FC of the created hydraulic fractures to the cumulative shale gas production volume from an unconventional reservoir. These models are interlinked in the sense that the output from the first model is the input to the second, and the output from the second model is the input to the third. A simplified design of the SIMS framework is shown in Fig. 3.4.

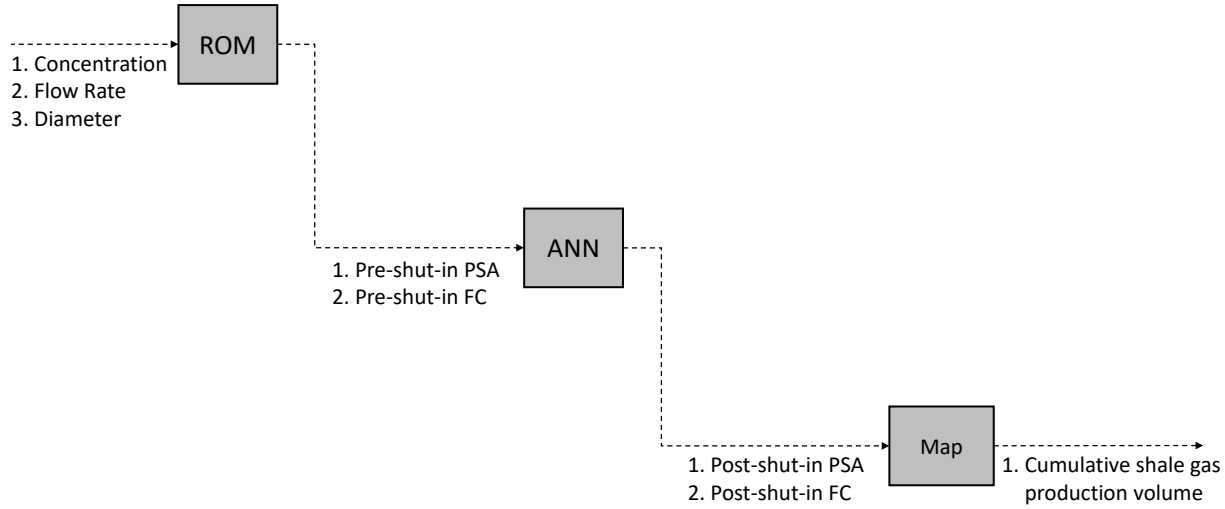

Figure 3.4: Illustration showing the proposed SIMS framework

The following subsections further elaborate each of these three models in detail.

3.4.1 Model 1: MOESP-based ROM to simulate hydraulic fracturing

Since it is computationally infeasible to directly use the UFM, Eqs. (2.1)–(2.8), we developed an MOESP-based ROM to describe the propagation, fluid flow and proppant transport phenomena for simultaneously propagating multiple fractures, which is given below:

$$x(t_{k+1}) = Ax(t_k) + Bu(t_k) \tag{3.1a}$$

$$y(t_k) = Cx(t_k) \tag{3.1b}$$

where $x(t_k)$ are the ROM states, $u(t_k) = [Q_{x0}(t_k), C_{x0}(t_k), D_{x0}(t_k)]^{\mathrm{T}}$ represent the input variables, $Q_{x0}(t_k)$, $C_{x0}(t_k)$ and $D_{x0}(t_k)$ are the fracturing fluid flow rate, proppant concentration and the injected proppant diameter, respectively, and the output variables, $y(t_k)$=[$PSA_{frac}(t_k)$, $Conductivity_{frac}(t_k)]^{\mathrm{T}}$, are the average PSA and average FC at the end of pumping. It is worthwhile to note that this model is only used to describe the hydraulic fracturing process until the end of pumping (i.e., pre-shut-in).

A training data set has been used to obtain the model parameters to be determined (i.e., $x(0)$, the initial estimate of the state, and the matrices A, B, and C) for a given order of the MOESP algorithm. Open-loop simulations were carried out using Mangrove and the data were used to create a 2^{nd} order linear time-invariant state-space model. The pumping schedule chosen for training the ROM is shown in Fig. 3.5.

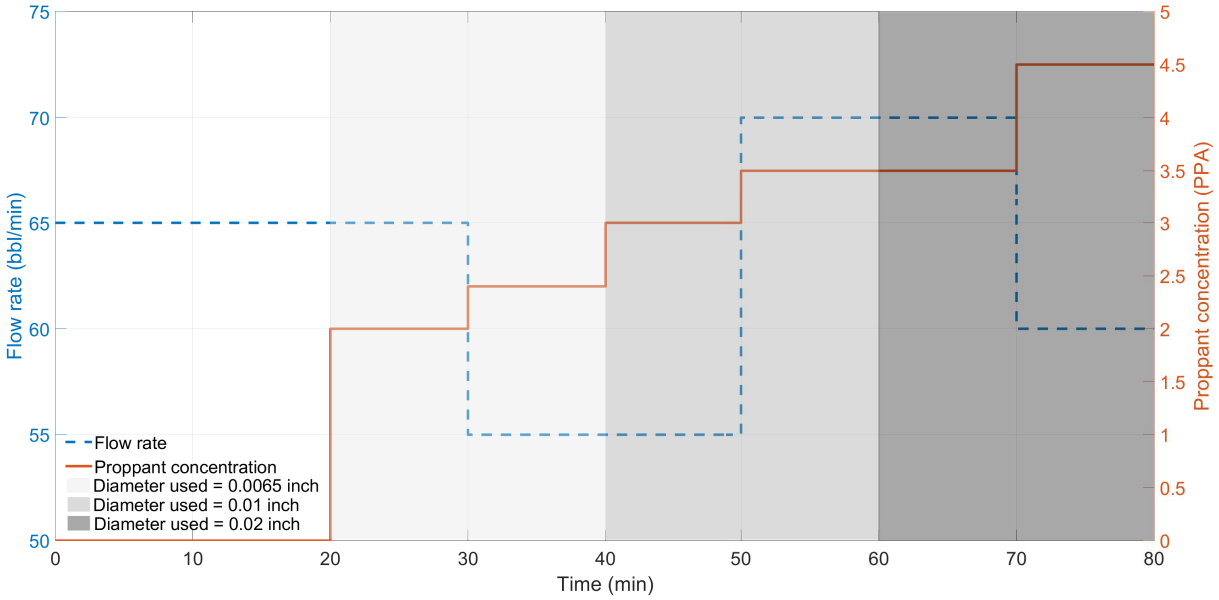

Figure 3.5: The pumping schedule used for training Model 1 (MOESP-based ROM)

This training input is chosen such that it satisfies the minimum and maximum practical fracturing fluid flow rate and proppant concentration. The proppant diameters chosen in the training input

pumping schedule are also ensured to follow a non-decreasing trend across the pumping stages, which is a common industry practice. Fig. 3.6 shows the training fit between the estimated average PSA and average FC values from the MOESP-based ROM and the corresponding values from Mangrove (i.e., high-fidelity model).

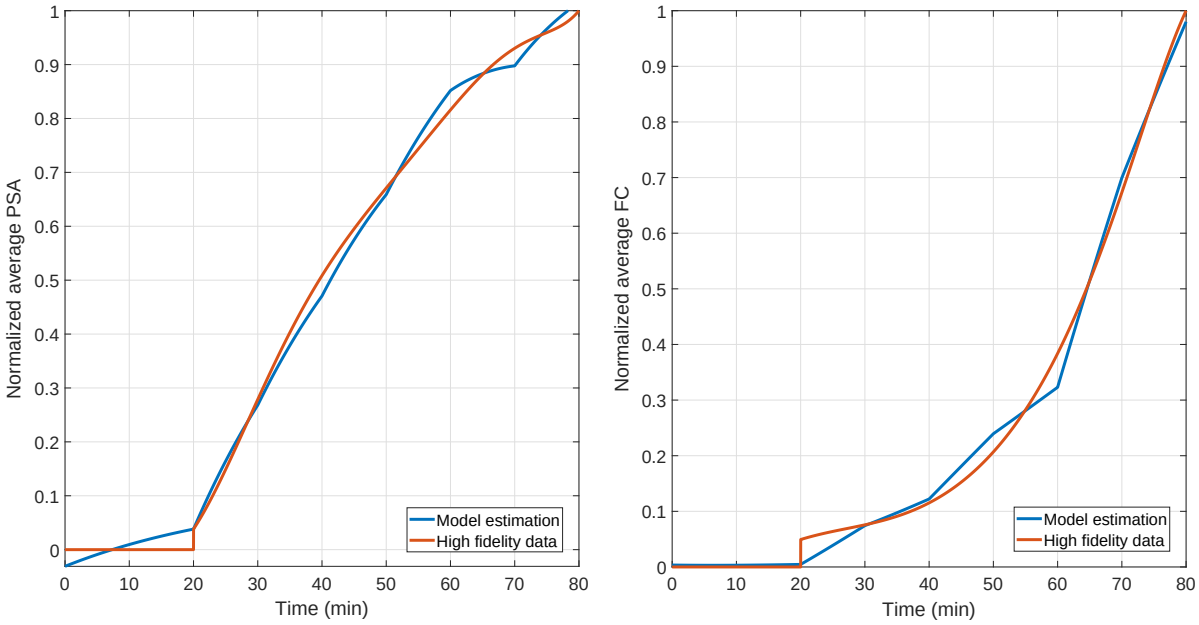

Figure 3.6: Training fit for Model 1 (MOESP-based ROM)

It is observed that the estimated average PSA and average FC converge quickly to the true values. The computational effort required to solve Eq. (3.1) is very small as compared to that of solving the UFM, Eqs. (2.1)–(2.8). The performance of the ROM has been validated by comparing it with a different testing pumping schedule within the practical considerations (Fig. 3.7).

Fig. 3.8 shows the comparison between the ROM and Mangrove. It can be clearly seen that the average PSA and average FC obtained from the ROM are close to the corresponding outputs obtained from Mangrove.

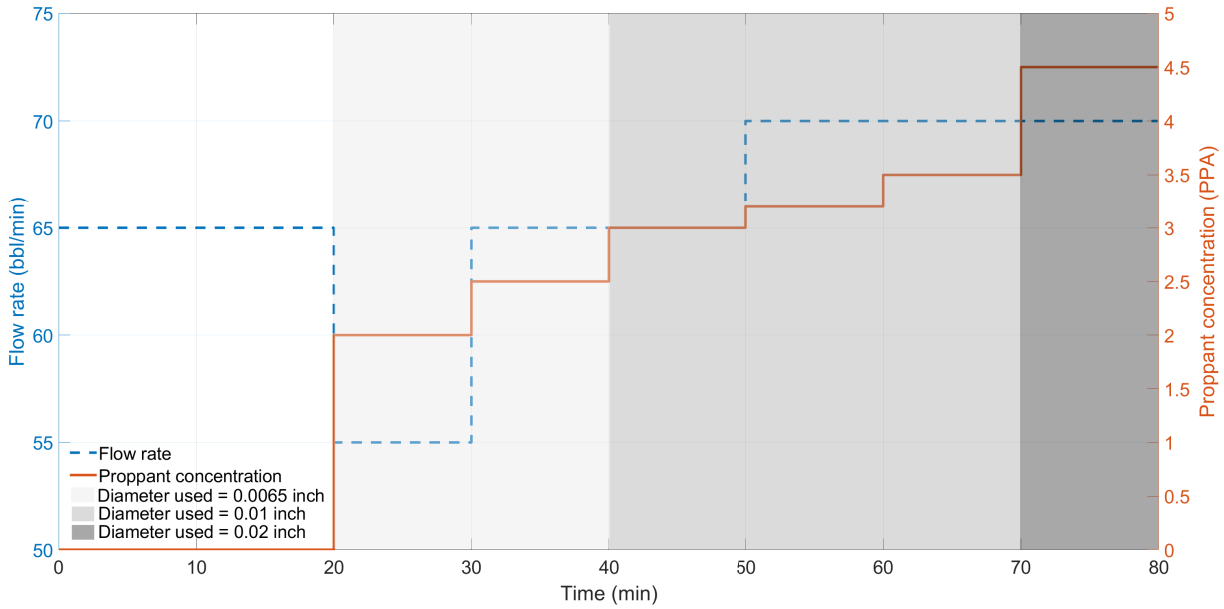

Figure 3.7: The pumping schedule used for validating Model 1 (MOESP-based ROM)

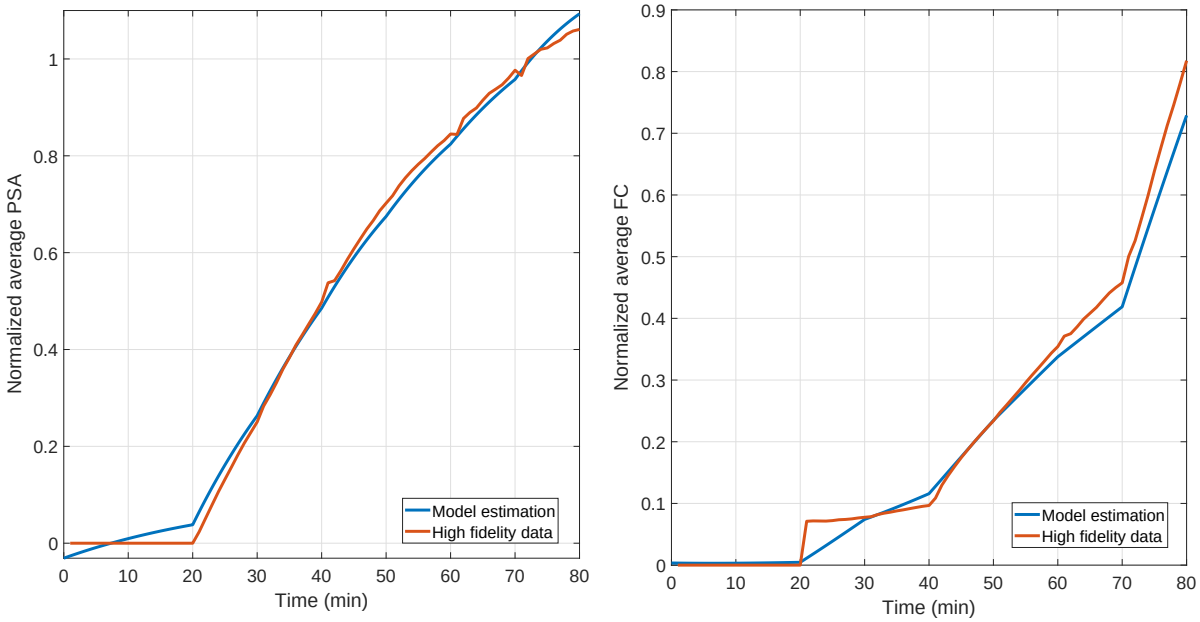

Figure 3.8: Validation fit for Model 1 (MOESP-based ROM)

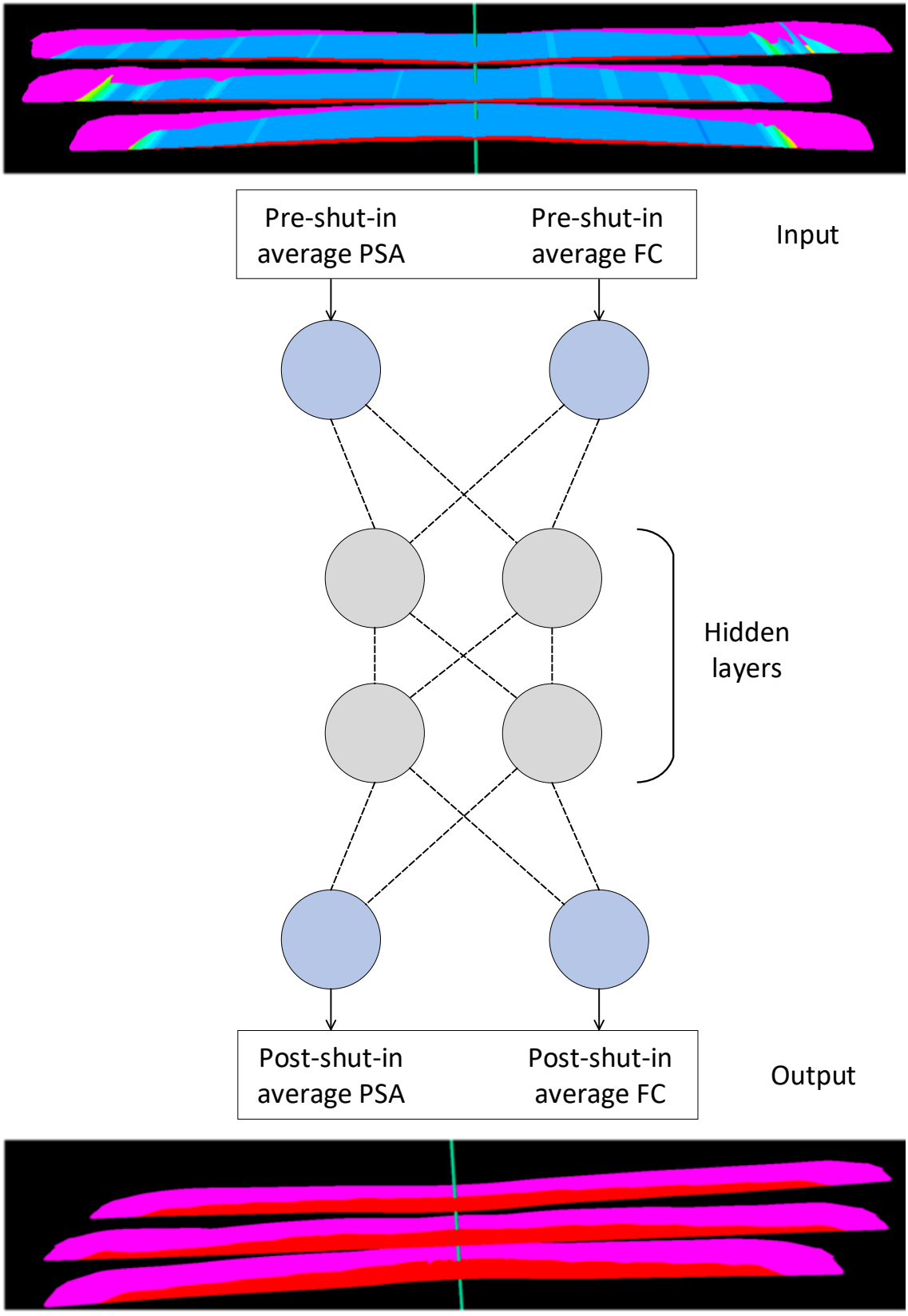

Figure 3.9: Illustration showing the basic structure of Model 2 (ANN)

3.4.2 Model 2: ANN-based model to simulate proppant settling

The second model in the SIMS framework is an ANN. This is an input-output model to capture the proppant settling dynamics in simultaneously propagating multiple fractures. At the end of pumping (i.e., pre-shut-in stage), the proppant in suspension starts settling down due to gravity. When the dynamic settling process has finally completed and reached an equilibrium (i.e., post-shut-in stage), a proppant bank is formed in the propped hydraulic fractures. This model takes the pre-shut-in average PSA and pre-shut-in average FC predicted from Model 1 as the two inputs and provides the post-shut-in average PSA and post-shut-in average FC of the propped hydraulic fractures as the two outputs. The network structure is designed to have two hidden layers, with two nodes in each hidden layer. This model is intermediate as it takes its inputs from Model 1 and passes on its outputs to Model 3, hence acting as a bridge between the other two models. A simplified illustration of the structure is shown in Fig. 3.9.

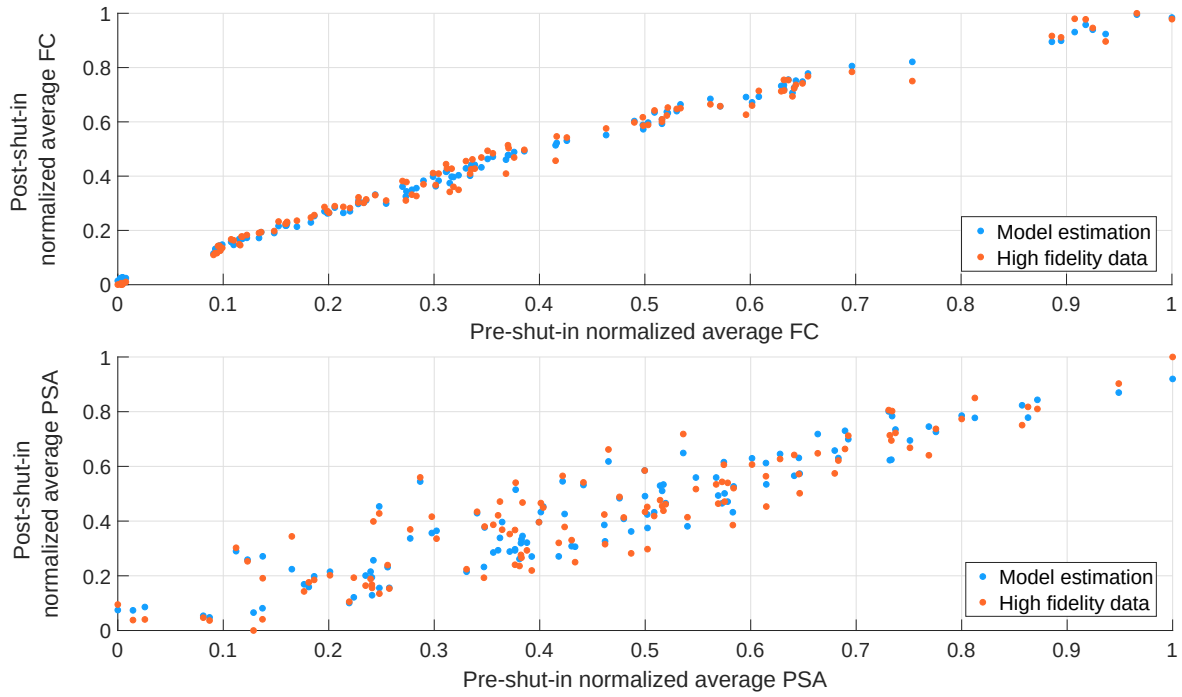

Figure 3.10: Scatter graph for training data used in Model 2 (ANN)

These training inputs and training outputs have been obtained by applying several different pumping schedules of a variety of proppant diameters, flow rates and concentrations to the UFM. The network has then been trained using Baysian Regularization method with sigmoidal activation functions. Specifically, 110 samples were used for training the network. Scatter-fit for the training samples for the proposed network can be seen from Fig. 3.10.

The trained ANN is then used to test 25 samples, which were not used during the training process. When this trained network was used on the test samples, the corresponding mean squared error (MSE) value was found to be 0.0045, which indicates a well-trained model. The scatter fit for the testing samples can be seen from Fig. 3.11.

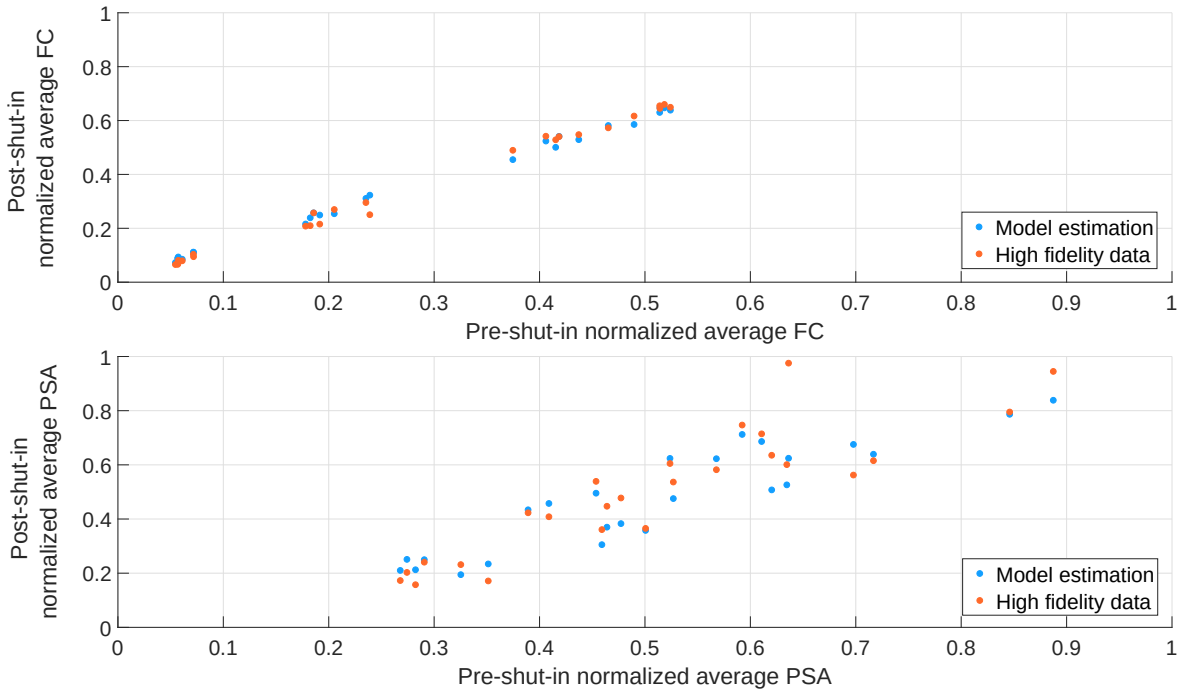

Figure 3.11: Scatter graph for validation data used in Model 2 (ANN)

3.4.3 Model 3: Map-based model to correlate propped fracture properties to gas production

The third model in SIMS framework is a map that has been generated using UFM (Mangrove) and INTERSECT Production Simulator. It has been generated using 86 pumping schedules, with

varying proppant concentration, fluid flow rates and proppant diameters. The model is based on the assumption that the cumulative shale gas production volume from an unconventional reservoir depends only on the average PSA and the average FC of propped fractures. The map is shown in Fig. 3.12. The x-axis in the map corresponds to average FC and the y-axis corresponds to the average PSA. The z-axis of the map denotes the cumulative amount of shale gas produced from the reservoir at the end of 10 years. It is worthwhile to note that since this final map linking propped fracture properties to the cumulative shale gas production volume is non-monotonic in nature, we proceeded with formulating an optimization problem to find a maximum in this region for a given amount of proppant to be injected, thereby corresponding to the case of maximum cumulative shale gas production at the end of 10 years.

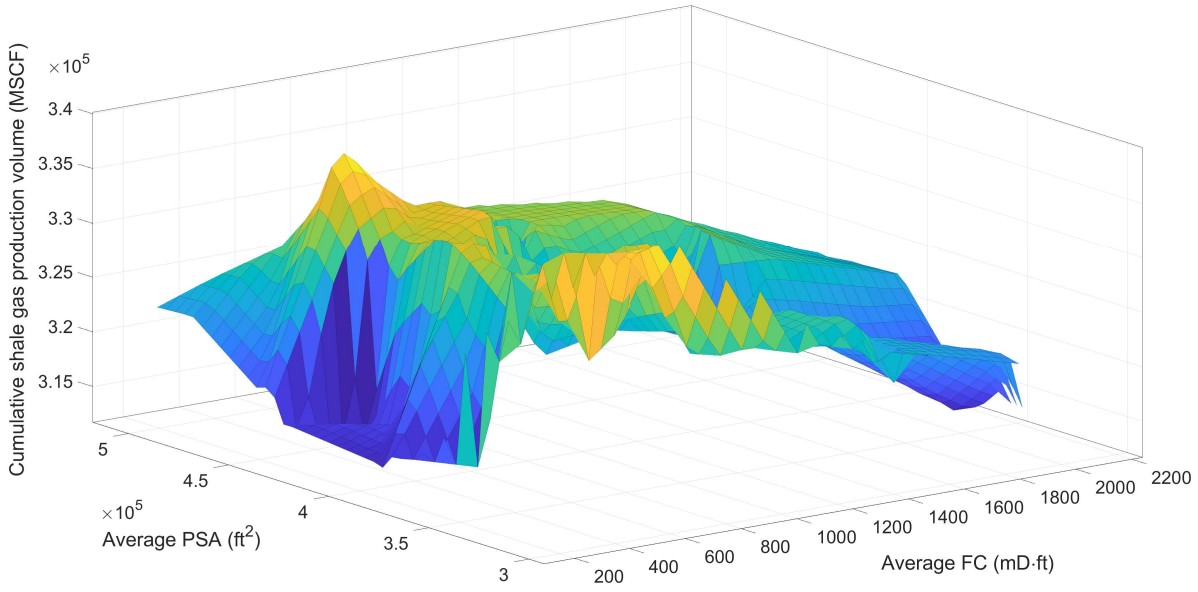

Figure 3.12: Illustration of Model 3 in the SIMS framework

3.5 Brief overview of existing pumping schedules

In this section, we present the various pumping schedule design techniques presently available in the literature.

One of the first attempts to design a pumping schedule was done by Nolte [43], where he developed a power-law type proppant concentration schedule. Despite being quite popular among researchers in academia as well as oil and gas industry since then, it has a few pragmatic restrictions: (1) it does not consider gravity-induced settling of the proppant; (2) it is only applicable to treatments leading to a single hydraulic fracture; (3) a plant-model mismatch might lead to premature stopping of the hydraulic fracture propagation; and (4) the pumping schedule is designed offline and applied in an open-loop manner to a hydraulic fracturing process.

Gu and Desroches [61] developed a pumping schedule generator using an iterative method to obtain the desired fracture length and proppant concentration (inverse problem) considering premature bridging and tip screenout. Another approach by Phatak et al. [62] studied the impact of fracturing fluid volume, proppant size, pumping rate, proppant concentration and proppant injection sequence on shale gas production rate. Later, Dontsov and Peirce [63] proposed a pumping schedule that has higher accuracy than Nolte [43] by assuming a weak impact of proppant particles on fracture propagation. However, they did not consider the impact of average PSA and average FC on shale gas production.

Recently, a new model-based controller was designed by Siddhamshetty et al. [1] to compute fracturing fluid pumping schedules online and to achieve an optimal fracture geometry by achieving a uniform proppant bank distribution at the end of pumping. They considered multiple simultaneously propagating fractures, and included stress shadow effects and proppant transport as well. Siddhamshetty et al. [49] further developed this approach for application to naturally fractured unconventional reservoirs. Specifically, in addition to proppant transport, stress shadow effects and simultaneously propagating multiple fractures, Siddhamshetty et al. [49] also included the presence of natural fractures and their interaction with the propagating hydraulic fractures, and developed a feedback control strategy to maximize the TFSA of the fracture network. However, they only considered the injection of a single-size proppant throughout the stages in their pumping schedule, and did not consider the effect of average PSA and average FC together on the shale oil and gas production.

In this work, we propose a multi-size proppant pumping schedule for simultaneously propagating multiple fractures. We assume the available proppant sizes to be restricted to three diameters- 0.0065 inch, 0.01 inch and 0.02 inch. As shown in the previous sections, since the inclusion of multiple proppant sizes is proposed, the objective can no longer be restricted to just maximizing the TFSA, because of a significant variation in the proppant conductivity across the different proppant sizes. Therefore, to take this variation into account, we propose a pumping schedule that maximizes shale gas production volume, which is a function of average PSA and average FC (Section 3.4). To achieve this objective, we have formulated an optimization problem in the following section. The SIMS framework proposed in Section 3.4 has been integrated within the proposed optimizer to compute a multi-size proppant pumping schedule to maximize cumulative shale gas production volume in an unconventional reservoir.

3.6 Formulation of optimization strategy using SIMS to maximize shale gas production in unconventional reservoirs

In this section, we present the design of an optimization problem to find a pumping schedule that maximizes the cumulative shale gas production volume at the end of 10 years in an unconventional reservoir, fractured using simultaneously propagating multiple fractures. We have utilized the three models in the proposed SIMS framework (Section 3.4) and solved the following optimization

problem to compute the optimal pumping schedule:

$$\max_{\substack{C_{stage,1},\ldots,C_{stage,8}\\ Q_{stage,1},\ldots,Q_{stage,8}\\ D_{stage,1},\ldots,D_{stage,8}}} \quad Gas_{frac}(C_{stage,m}, Q_{stage,m}, D_{stage,m}) \tag{3.2a}$$

$$\text{s.t.} \quad \text{Model 1 (Section 3.4.1)} \tag{3.2b}$$

$$\text{Model 2 (Section 3.4.2)} \tag{3.2c}$$

$$\text{Model 3 (Section 3.4.3)} \tag{3.2d}$$

$$C_{stage,m-1} \leq C_{stage,m} \leq 5 \text{ PPA} \tag{3.2e}$$

$$Q_{min} \leq Q_{stage,m} \leq Q_{max} \tag{3.2f}$$

$$D_{stage,m} \in \{0.0065 \text{ inch}, 0.01 \text{ inch}, 0.02 \text{ inch}\} \tag{3.2g}$$

$$m = 1, \ldots, 8 \tag{3.2h}$$

$$\Delta \left(\sum_{m=1}^{8} Q_{stage,m} C_{stage,m} \right) = M_{prop} \tag{3.2i}$$

where Δ denotes the duration of each sampling time, Gas_{frac} is the cumulative volume of shale gas produced at the end of 10 years, the decision variables $C_{stage,m}$, $Q_{stage,m}$ and $D_{stage,m}$ are the concentration, flow rate and the diameter of the injected proppant at the m^{th} stage, respectively. Throughout this work, we assume pumping schedules to have a total of 8 pumping stages, each of 10 mins duration.

In the optimization problem of Eq. (3.2), Eqs. (3.2e)-(3.2h) are the constraints on the decision variables (i.e. fracturing fluid flow rate injected at the wellbore, proppant concentration, and diameter of the proppant). The proppant diameters are chosen in non-decreasing order. The units of fracturing fluid flow rate, proppant concentration and proppant diameter are $\mathrm{bbl/min}$, PPA (1 pound of the proppant added to one gallon of fracturing fluid) and inch, respectively. The total amount of proppant injected is equal to 400000 lb, constrained using Eq. (3.2i). The optimization problem has been solved for the following three cases. In Case A, the optimization problem was solved using all the three models of the SIMS framework. In Case B, we assume a 'conductivity-

specific' reservoir treatment, where the optimization objective is only to maximize the post-shut-in average FC of the reservoir. Thus, this would require only the first two models of the SIMS framework. In Case C, we assume a 'surface area- specific' reservoir treatment, where the optimization objective is only to maximize the post-shut-in average PSA. Similar to Case B, this would also require only the first two models of the SIMS framework.

3.7 Optimization results under the proposed framework

In this section, we present optimization results to signify the performance of our proposed optimizer using the SIMS framework developed in Section 3.4. Mangrove, described in Section 2.2, has been used as a high-fidelity simulator for a hydraulic fracturing operation resulting in simultaneously propagating multiple fractures.

3.7.1 Optimization results for case studies

In Case A, the total proppant amount considered is $M_{prop} = 400000\,\mathrm{lb}$. Using the three models incorporated in the SIMS framework, the proposed optimizer in Section 3.6 computed the pumping schedule to maximize the cumulative shale gas production volume, 10 years after initiation of the hydraulic fracturing operation. The pumping schedule obtained from the optimizer is shown in Fig. 3.13. When this pumping schedule was applied to the high-fidelity model, the average PSA and average FC values obtained were 355398 ft^2 and 679 $\mathrm{mD{\cdot}ft}$, respectively. The cumulative gas production volume at the end of 10 years was 330036 MSCF. In Case B, the total proppant amount considered is $M_{prop} = 400000\,\mathrm{lb}$. However, since the objective was chosen to maximize the average FC of the propped fractures, only Model 1 and Model 2 of the SIMS framework were incorporated into the optimization problem, Eq. (3.2). For this case, the pumping schedule obtained is shown in Fig. 3.14. When this pumping schedule was applied to the high-fidelity model, the average PSA and average FC values were 314789 ft^2 and 1983 $\mathrm{mD{\cdot}ft}$, respectively. The cumulative shale gas production volume at the end of 10 years was 317263 MSCF. In Case C, we assumed a total proppant amount of $M_{prop} = 400000\,\mathrm{lb}$, similar to Case A and Case B. Since the objective was chosen to maximize the average PSA of the propped fractures, we included only

Model 1 and Model 2 into the optimizer, Eq. (3.2). For this case, the pumping schedule obtained is shown in Fig. 3.15. When this pumping schedule was applied to the high-fidelity model, the average PSA and average FC values were 409035 ft^2 and 181 $\mathrm{mD{\cdot}ft}$, respectively. The cumulative gas production volume at the end of 10 years was 316059 MSCF.

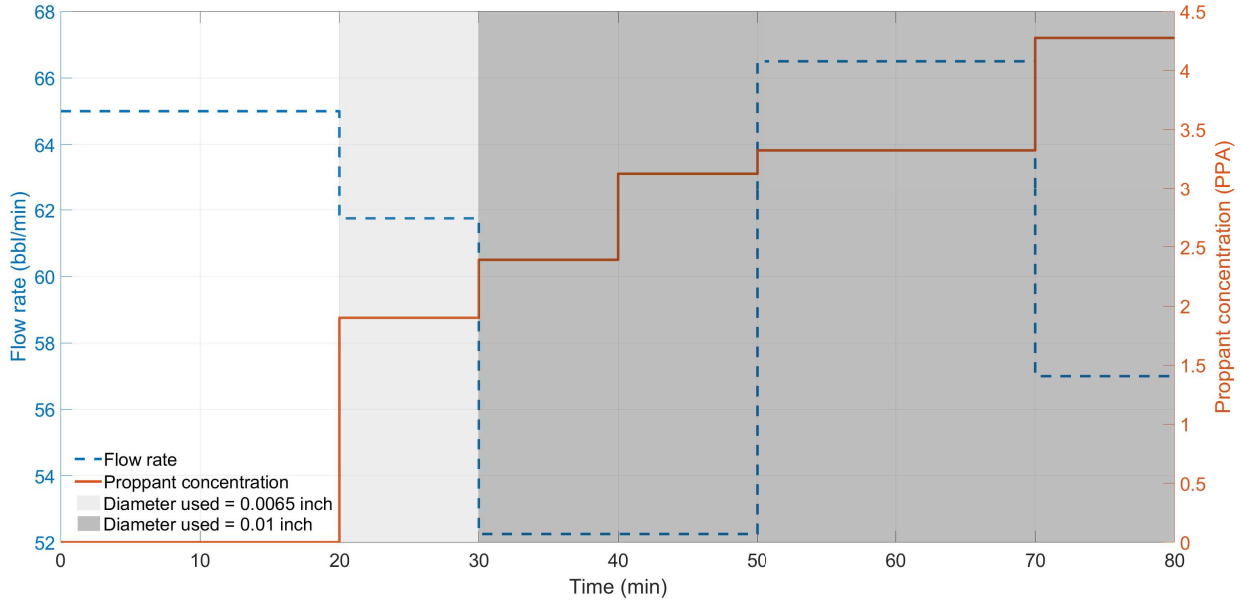

Figure 3.13: The pumping schedule obtained from the optimizer, Eq. (3.2), for Case A

Table 3.1 summarizes the results obtained after solving the optimization problem, Eq. (3.2). The pumping schedule obtained in Case A maximizes the cumulative shale gas production volume for a general case, where the effect of average PSA and average FC is coupled. We have also presented two other cases that provide pumping schedules aimed at maximizing cumulative shale gas production volume by either considering average FC or average PSA separately. From the pumping schedule results, we can clearly see that average FC is maximized in Case B, when all the stages in the pumping schedule have the largest proppant (i.e., 0.02 inch). Meanwhile, the average PSA is maximized in Case C, when the smallest proppant (i.e., 0.0065 inch) is injected throughout the pumping schedule. However, Case A, where average PSA and average FC are considered to-

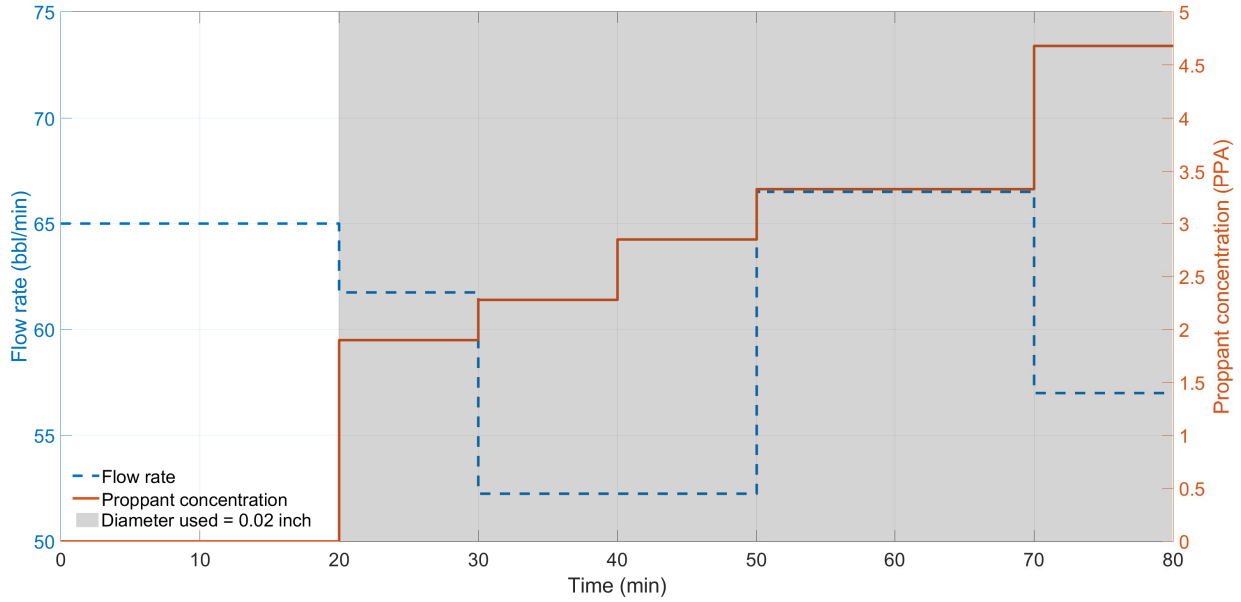

Figure 3.14: The pumping schedule obtained from the optimizer, Eq. (3.2), for Case B

gether, gives the maximum cumulative shale gas production volume in an unconventional reservoir considering simultaneously propagating multiple fractures. These results are in agreement with the analysis presented in Section 3.3.

Optimization Case	Average PSA (ft^2)	Average FC ($mD{\cdot}ft$)	Cumulative shale gas production volume (MSCF)
A	355398	679	330036
B	314789	1983	317263
C	409035	181	316059

Table 3.1: Simulation results after applying the output obtained from the optimizer, Eq. (3.2), to the high-fidelity model described in Section 2.2

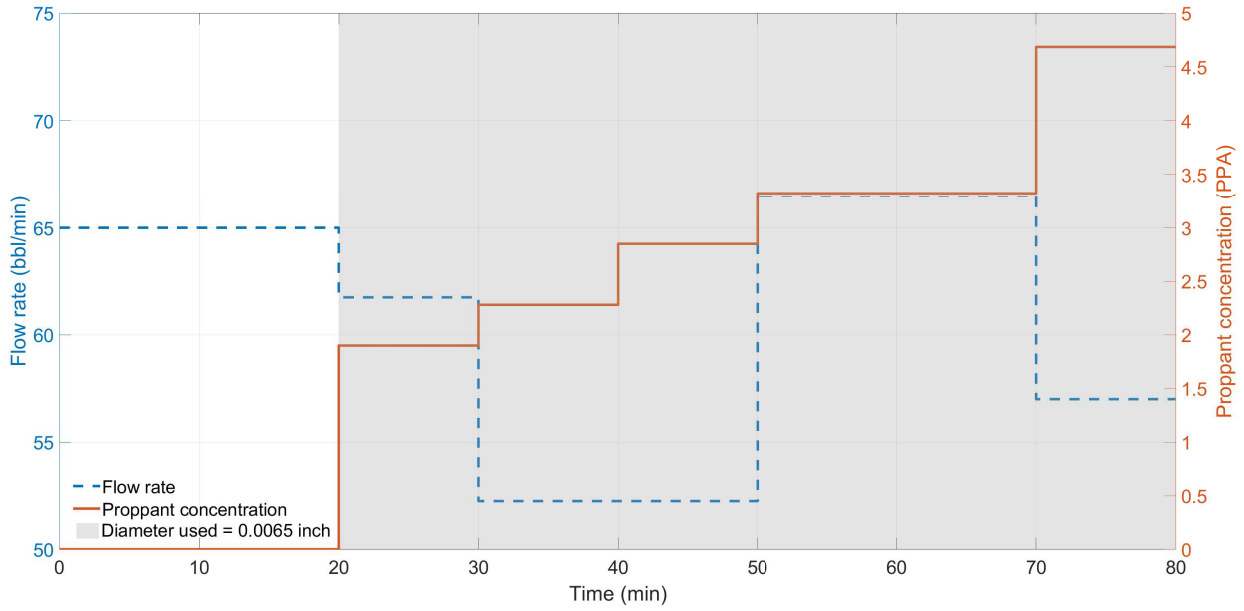

Figure 3.15: The pumping schedule obtained from the optimizer, Eq. (3.2), for Case C

3.7.2 Comparison with existing work

In this work, we have used Nolte's pumping schedule described in Section 2.4 for comparison with the output of the proposed optimizer. The pumping schedule is shown in Fig. 3.16.

This pumping schedule was applied to the high-fidelity model and the results obtained were compared with Case A, as shown in Table 3.2.

Pumping schedule	Average PSA (ft^2)	Average FC ($mD{\cdot}ft$)	Cumulative shale gas production volume (MSCF)
Case A	355398	679	330036
Nolte (1986)	439377	190	311896

Table 3.2: Comparison of average PSA, average FC, cumulative shale gas production volume from Case A and Nolte's pumping schedule

From the results, we can see that the pumping schedule obtained from Case A, Eq. (3.2), gives

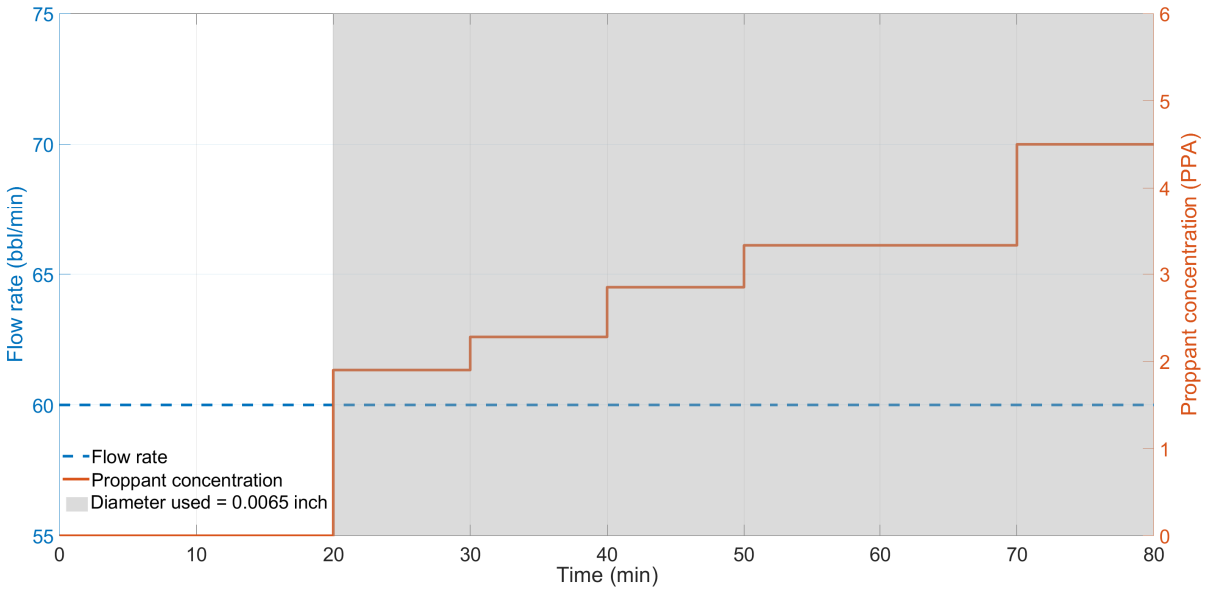

Figure 3.16: Nolte's pumping schedule used in this work

a cumulative shale gas production volume more than that of Nolte's schedule.

All the calculations, including model training, validation and deployment in the optimization problem were facilitated using MATLAB R2018b on a Dell workstation, powered by Intel(R) Core(TM) i7-4790 CPU@3.60GHz, running on the Windows 10 OS.

4. CONCLUSIONS

In this thesis, we developed optimal pumping schedules to enhance shale oil and gas production from unconventional reservoirs.

First, in Chapter 2, it was observed from the sensitivity analysis that the cumulative oil production from a well is proportional to TFSA, which in-turn depends on the fracturing fluid pumping schedule for given fracturing resources and natural fracture distributions. Therefore, we developed a novel MPC framework to compute the fracturing fluid pumping schedule that maximizes the TFSA in naturally fractured unconventional reservoirs. Initially, we constructed a ROM using the simulation data generated from Mangrove by considering the complex fracture growth in naturally fractured unconventional reservoirs. Then, the developed ROM was used for state estimation using a Kalman filter and available measurements. Next, a real-time MPC framework was developed utilizing the ROM and Kalman filter to compute the pumping schedule that maximizes the TFSA. Simulation results presented in Chapter 2 show that the maximum TFSA will lead to an oil production rate greater than those of the existing pumping schedules which were developed without considering natural fractures.

Then, in Chapter 3, we designed a multi-size proppant pumping schedule for the case of simultaneously propagating multiple fractures to maximize cumulative shale gas production volume from unconventional reservoirs. From the sensitivity analysis, we found out that the pumping schedule used for hydraulic fracturing determines the average PSA and average FC of the propped fractures, which in-turn are two useful parameters that determine the cumulative shale gas production volume from an unconventional reservoir. Therefore, we developed SIMS, a framework that links the pumping schedule parameters to the cumulative gas production volume. In this framework, we first developed a MOESP-based ROM to accurately represent the fracturing process. Then, an ANN was trained and tested to model the proppant settling process. The final model developed in SIMS is a map that was generated using the reservoir simulator to obtain the cumulative shale gas produced at the end of 10 years using the average PSA and average FC for an

unconventional reservoir. Finally, we proposed a framework to maximize the cumulative shale gas production volume by computing pumping schedules (i.e., flow rate, proppant concentration, and proppant diameter at the wellbore) using offline optimization techniques. Simulation results presented in this work include the pumping schedule obtained from the optimizer that maximizes the cumulative shale gas production volume at the end of 10 years for the three different case studies. Case A, where average PSA and average FC were considered together, gave the maximum cumulative shale gas production volume. When the pumping schedule obtained in Case A was compared with Nolte's schedule, the latter was found to give a less cumulative gas production volume than Case A.

In this thesis, pumping schedules were developed that enhance oil and gas production from unconventional reservoirs. We also demonstrated that when compared with existing pumping schedules, the pumping schedules proposed in this thesis resulted in higher cumulative oil and gas production volumes from unconventional reservoirs.

REFERENCES

[1] P. Siddhamshetty, K. Wu, and J. S. Kwon, "Modeling and control of proppant distribution of multi-stage hydraulic fracturing in horizontal shale wells," *Ind. & Eng. Chem. Res.*, vol. 58, pp. 3159–3169, 2019.

[2] C. Fredd, S. McConnell, C. Boney, and K. England, "Experimental study of hydraulic fracture conductivity demonstrates the benefits of using proppants," *In SPE Rocky Mountain Regional/Low-Permeability Reservoirs Symposium and Exhibition (SPE 60326), Denver, CO*, 2000.

[3] S. C. Maxwell, T. I. Urbancic, N. Steinsberger, and R. Zinno, "Microseismic imaging of hydraulic fracture complexity in the barnett shale," *In SPE Annual Technical Conference and Exhibition (SPE 77440), San Antonio, TX*, 2002.

[4] J. L. Daniels, G. A. Waters, J. H. Le Calvez, D. Bentley, and J. T. Lassek, "Contacting more of the barnett shale through an integration of real-time microseismic monitoring, petrophysics, and hydraulic fracture design," *In SPE Annual Technical Conference and Exhibition (SPE 110562), Anaheim, CA*, 2007.

[5] J. Gale, R. Reed, and J. Holder, "Natural fractures in the Barnett Shale and their importance for hydraulic fracture treatments," *AAPG Bull*, vol. 91, pp. 603–622, 2007.

[6] J. Gale, S. Laubach, J. Olson, P. Eichhubl, and A. Fall, "Natural fractures in shale: a review and new observations," *AAPG Bull*, vol. 98, pp. 2165–2216, 2014.

[7] A. Dahi-Taleghani and J. E. Olson, "How natural fractures could affect hydraulic-fracture geometry," *SPE Journal*, vol. 19, pp. 161–171, 2013.

[8] R. Yang, Z. Huang, W. Yu, G. Li, W. Ren, L. Zuo, X. Tan, K. Sepehrnoori, S. Tian, and M. Sheng, "A comprehensive model for real gas transport in shale formations with complex non-planar fracture networks," *Scientific Reports*, vol. 6, p. 36673, 2016.

[9] T. Blanton, "Propagation of hydraulically and dynamically induced fractures in naturally fractured reservoirs," *In SPE Unconventional Gas Technology Symposium (SPE 15261), Louisville, KY*, 1986.

[10] N. Warpinski and L. Teufel, "Influence of geologic discontinuities on hydraulic fracture propagation," *Journal of Petroleum Technology*, vol. 39, pp. 209–220, 1987.

[11] C. Renshaw and D. Pollard, "An experimentally verified criterion for propagation across unbounded frictional interfaces in brittle, linear elastic materials," *In International Journal of Rock Mechanics and Mining Sciences & Geomechanics Abstracts*, vol. 32, pp. 237–249, 1995.

[12] A. Dahi-Taleghani and J. E. Olson, "Numerical modeling of multistranded hydraulic fracture propagation: accounting for the interaction between induced and natural fractures," *In SPE Annual Technical Conference Conference and Exhibition (SPE 124884), New Orleans, LA*, 2009.

[13] W. Wang, J. E. Olson, and M. Prodanovic, "Natural and hydraulic fracture interaction study based on semi-circular bending experiments," *In Unconventional Resources Technology Conference (SPE 168714), Denver, CO*, 2013.

[14] W. Xu, J. H. Le Calvez, and M. J. Thiercelin, "Characterization of hydraulically-induced fracture network using treatment and microseismic data in a tight-gas sand formation: a geomechanical approach," *In SPE Tight Gas Completions Conference (SPE 125237), San Antonio, TX*, 2009.

[15] W. Xu, M. J. Thiercelin, U. Ganguly, X. Weng, H. Gu, H. Onda, J. Sun, and J. Le Calvez, "Wiremesh: a novel shale fracturing simulator," *In International Oil and Gas Conference and Exhibition in China (SPE 132218), Beijing, China*, 2010.

[16] B. R. Meyer and L. W. Bazan, "A discrete fracture network model for hydraulically induced fractures-theory, parametric and case studies," *In SPE Hydraulic Fracturing Technology Conference (SPE 140514), The Woodlands, TX*, 2011.

[17] J. E. Olson and A. D. Taleghani, "Modeling simultaneous growth of multiple hydraulic fractures and their interaction with natural fractures," *In SPE Hydraulic Fracturing Technology Conference (SPE 119739), The Woodlands, TX*, 2009.

[18] E. Budyn, G. Zi, N. Moes, and T. Belytschko, "A method for multiple crack growth in brittle materials without remeshing," *International Journal for Numerical Methods in Engineering*, vol. 61, pp. 1741–1770, 2004.

[19] R. Keshavarzi, S. Mohammadi, and H. Bayesteh, "Hydraulic fracture propagation in unconventional reservoirs: the role of natural fractures," *In 46th US Rock Mechanics/Geomechanics Symposium (ARMA-2012-129), Chicago, IL*, 2012.

[20] K. Wu and J. Olson, "Mechanics analysis of interaction between hydraulic and natural fractures in shale reservoirs," *In Unconventional Resources Technology Conference, Denver,*, vol. CO, pp. 1824–1841, 2014.

[21] H. Gu and X. Weng, "Criterion for fractures crossing frictional interfaces at non-orthogonal angles," *In 44th US Rock Mechanics Symposium and 5th US-Canada Rock Mechanics Symposium (ARMA-10-198), Salt Lake City, UT*, 2010.

[22] X. Weng, O. Kresse, D. Chuprakov, C. E. Cohen, R. Prioul, and U. Ganguly, "Applying complex fracture model and integrated workflow in unconventional reservoirs," *Journal of Petroleum Science and Engineering*, vol. 124, pp. 468–483, 2014.

[23] P. Siddhamshetty, S. Liu, P. P. Valkó, and J. S. Kwon, "Feedback control of proppant bank heights during hydraulic fracturing for enhanced productivity in shale formations," *AIChE Journal.*, vol. 64, pp. 1638–1650, 2017.

[24] Q. Gu and K. A. Hoo, "Evaluating the performance of a fracturing treatment design," *Ind. & Eng. Chem. Res*, vol. 53, pp. 10491–10503, 2014.

[25] A. Narasingam, P. Siddhamshetty, and J. S. Kwon, "Temporal clustering for order reduction of nonlinear parabolic PDE systems with time-dependent spatial domains: Application to a hydraulic fracturing process," *AIChE Journal*, vol. 63, pp. 3818–3831, 2017.

[26] A. Narasingam, P. Siddhamshetty, and J. S. Kwon, "Handling spatial heterogeneity in reservoir parameters using proper orthogonal decomposition based ensemble kalman filter for model-based feedback control of hydraulic fracturing," *Ind. & Eng. Chem. Res.*, vol. 57, pp. 3977–3989, 2018.

[27] H. S. Sidhu, P. Siddhamshetty, and J. S. Kwon, "Approximate dynamic programming based control of proppant concentration in hydraulic fracturing," *Mathematics*, vol. 6, p. 132, 2018.

[28] S. Yang, P. Siddhamshetty, and J. S. Kwon, "Optimal pumping schedule design to achieve a uniform proppant concentration level in hydraulic fracturing," *Computers & Chemical Engineering*, vol. 101, pp. 138–147, 2017.

[29] P. Siddhamshetty, K. Wu, and J. S. Kwon, "Optimization of simultaneously propagating multiple fractures in hydraulic fracturing to achieve uniform growth using data-based model reduction," *Chemical Engineering Research and Design*, vol. 136, pp. 675–686, 2018.

[30] P. Siddhamshetty, S. Yang, and J. S. Kwon, "Modeling of hydraulic fracturing and designing of online pumping schedules to achieve uniform proppant concentration in conventional oil reservoirs," *Computers & Chemical Engineering*, vol. 114, pp. 306–317, 2018.

[31] P. Siddhamshetty and J. S. Kwon, "Simultaneous measurement uncertainty reduction and proppant bank height control of hydraulic fracturing," *Computers & Chemical Engineering*, vol. 127, pp. 272–281, 2019.

[32] H. S. Sidhu, A. Narasingam, P. Siddhamshetty, and J. S. Kwon, "Model order reduction of nonlinear parabolic PDE systems with moving boundaries using sparse proper orthogonal decomposition: Application to hydraulic fracturing," *Computers & Chemical Engineering*, vol. 112, pp. 92–100, 2018.

[33] K. Wu and J. E. Olson, "Numerical investigation of complex hydraulic-fracture development in naturally fractured reservoirs," *SPE Production & Operations*, vol. 31, pp. 300–309, 2016.

[34] M. G. Mack, J. L. Elbel, and A. R. Piggott, "Numerical representation of multilayer hydraulic fracturing," *In The 33th US Symposium on Rock Mechanics (ARMA-92-0335), Santa Fe, NM*, 1992.

[35] P. Valko and M. J. Economides, *Hydraulic fracture mechanics.* Chichester: Wiley, 1995.

[36] D. Chuprakov, O. Melchaeva, and R. Prioul, "Hydraulic fracture propagation across a weak discontinuity controlled by fluid injection," *In ISRM International Conference for Effective and Sustainable Hydraulic Fracturing (ISRM-ICHF-2013-008), Brisbane, Australia*, 2013.

[37] D. Chuprakov, O. Melchaeva, and R. Prioul, "Injection-sensitive mechanics of hydraulic fracture interaction with discontinuities," *Rock Mechanics and Rock Engineering*, vol. 47, pp. 1625–1640, 2014.

[38] S. L. Crouch, A. M. Starfield, and F. J. Rizzo, "Boundary element methods in solid mechanics," *Journal of Applied Mechanics*, vol. 50, p. 704, 1983.

[39] J. E. Olson, "Multi-fracture propagation modeling: Applications to hydraulic fracturing in shales and tight gas sands," *In The 42nd US Symposium on Rock Mechanics (ARMA-08-327), San Francisco, CA*, 01 2008.

[40] C. L. Cipolla, T. Fitzpatrick, M. J. Williams, and U. K. Ganguly, "Seismic-to-simulation for unconventional reservoir development," *In SPE Reservoir Characterisation and Simulation Conference and Exhibition (SPE 146876), Abu Dhabi, UAE*, 2011.

[41] H. Gu, X. Weng, J. B. Lund, M. G. Mack, U. Ganguly, and R. Suarez-Rivera, "Hydraulic fracture crossing natural fracture at non-orthogonal angles, a criterion, its validation and applications," *In SPE Hydraulic Fracturing Technology Conference (SPE 139984), The Woodlands,*, vol. TX, 2011.

[42] X. Weng, O. Kresse, C. E. Cohen, R. Wu, and H. Gu, "Modeling of hydraulic fracture network propagation in a naturally fractured formation," *In SPE Hydraulic Fracturing Technology Conference (SPE 140253), The Woodlands, TX*, 11 2011.

[43] K. G. Nolte, "Determination of proppant and fluid schedules from fracturing-pressure decline," *SPE Production Engineering*, vol. 1, pp. 255–265, 1986.

[44] Y. K. Sukkar and D. Cornell, "Direct calculation of bottom-hole pressures in natural gas wells," *Society of Petroleum Engineers*, vol. 204, pp. 43–48, 1955.

[45] N. R. Warpinski, L. G. Griffin, E. J. Davis, and T. Grant, "Improving hydraulic fracture diagnostics by joint inversion of downhole microseismic and tiltmeter data," *In SPE Annual Technical Conference and Exhibition (SPE 102690), San Antonio, TX*, 2006.

[46] Q. Gu and K. A. Hoo, "Model-based closed-loop control of the hydraulic fracturing process," *Ind. & Eng. Chem. Res.*, vol. 54, pp. 1585–1594, 2015.

[47] K. D. Scott, W. C. Chu, and R. W. Flumerfelt, "Application of real-time bottom-hole pressure to improve field development strategies in the midland basin wolfcamp shale," *In Unconventional Resources Technology Conference, San Antonio, TX*, 2015.

[48] Z. Sun, Q. Gu, and J. Dykstra, "Uncertainty reduction of hydraulic fracturing process," *In American Control Conference, Boston, MA*, 2016.

[49] P. Siddhamshetty, P. Bhandakkar, and J. S. Kwon, "Enhancing total fracture surface area in naturally fractured unconventional reservoirs via model predictive control," *Journal of Petroleum Science and Engineering*, vol. 184, p. 106525, 2020.

[50] R. F. Westwood, S. M. Toon, and N. J. Cassidy, "A sensitivity analysis of the effect of pumping parameters on hydraulic fracture networks and local stresses during shale gas operations," *Fuel*, vol. 203, pp. 843–852, 2017.

[51] H. A. Wahl, "Horizontal fracture design based on propped fracture area," *Journal of Petroleum Technology*, vol. 17, pp. 723 – 730, 1965.

[52] M. Ramurthy, R. D. Barree, D. P. Kundert, J. E. Petre, and M. J. Mullen, "Surface-area vs. conductivity-type fracture treatments in shale reservoirs," *In SPE Hydraulic Fracturing Technology Conference, The Woodlands, TX*, 2011.

[53] D. Schmidt, P. R. Rankin, B. Williams, T. Palisch, and J. Kullman, "Performance of mixed proppant sizes," *In SPE Hydraulic Fracturing Technology Conference (SPE 168629), The Woodlands, TX*, 2014.

[54] J. Zhang, "Theoretical conductivity analysis of surface modification agent treated proppant," *Fuel*, vol. 134, pp. 166–170, 2014.

[55] W. Yu, T. Zhang, S. Du, and K. Sepehrnoori, "Numerical study of the effect of uneven proppant distribution between multiple fractures on shale gas well performance," *Fuel*, vol. 142, pp. 189–198, 2015.

[56] S. Tong and K. Mohanty, "Proppant transport study in fractures with intersections," *Fuel*, vol. 181, pp. 463–477, 2016.

[57] J. Zeng, H. Li, and D. Zhang, "Numerical simulation of proppant transport in propagating fractures with the multi-phase particle-in-cell method," *Fuel*, vol. 245, pp. 316–335, 2019.

[58] X. Hu, K. Wu, G. Li, J. Tang, and Z. Shen, "Effect of proppant addition schedule on the proppant distribution in a straight fracture for slickwater treatment," *Journal of Petroleum Science and Engineering*, vol. 167, pp. 110–119, 03 2018.

[59] D. Fan and A. Tavakkol, "Semi-analytical modeling of shale gas flow through fractal induced fracture networks with microseismic data," *Fuel*, vol. 193, pp. 444–459, 2017.

[60] P. Ghahri, M. Jamiolahmadi, E. Alatefi, D. Wilkinson, F. Sedighi, and H. Hamidi, "A new and simple model for the prediction of horizontal well productivity in gas condensate reservoirs," *Fuel*, vol. 223, pp. 431–450, 2018.

[61] H. Gu and J. Desroches, "New pump schedule generator for hydraulic fracturing treatment design," *SPE Latin American and Caribbean Petroleum Engineering Conference, Port-of-Spain, Trinidad and Tobago*, 2003.

[62] A. Phatak, O. Kresse, O. V. Nevvonen, C. Abad, C.-e. Cohen, V. Lafitte, P. Abivin, X. Weng, and K. W. England, "Optimum fluid and proppant selection for hydraulic fracturing in shale

gas reservoirs: a parametric study based on fracturing-to-production simulations," *In SPE Hydraulic Fracturing Technology Conference (SPE 163876), The Woodlands, TX*, 2013.

[63] E. V. Dontsov and A. P. Peirce, "A new technique for proppant schedule design," *Hydraulic Fracturing Journal*, vol. 1, pp. 1–8, 2014.